EFFECT OF NANOCLAY ON THE MORPHOLOGICAL PROPERTIES OF POLY (ETHYLENE TEREPHTHALATE) IN RELATION TO FRACTURE TOUGHNESS

Siddhi Pendse

Thesis Prepared for the Degree of

MASTER OF SCIENCE

UNIVERSITY OF NORTH TEXAS

August 2005

APPROVED:

Nandika D'Souza, Major Advisor
Mike Kaufman, Committee Member and Chair of the Department of Materials Science and Engineering
Witold Brostow, Committee Member
Oscar Garcia, Dean of College of Engineering
Sandra L. Terrell, Dean of the Robert B. Toulouse School of Graduate Studies

Pendse, Siddhi. *Morphological properties of poly (ethylene terephthalate) (PET) nanocomposites in relation to fracture toughness*. Master of Science (Material Science and Engineering), August 2005, 84 pg, 7 tables, 33 illustrations, references.

The effect of incorporation of montmorillonite layered silicate (MLS) on poly (ethylene terephthalate) (PET) matrix was investigated. MLS was added in varying concentration of 1 to 5 weight percent in the PET matrix. DSC and polarized optical microscopy were used to determine the crystallization effects of MLS addition. Non isothermal crystallization kinetics showed that the melting temperature and crystallization temperature decrease as the MLS percent increases. This delayed crystallization along with the irregular spherulitic shape indicates hindered crystallization in the presence of MLS platelets. The influence of this morphology was related with the fracture toughness of PET nanocomposites using essential work of fracture coupled with the infra red (IR) thermography. Both the essential as well as non essential work of fracture decreased on addition of MLS with nanocomposite showing reduced toughness.

ACKNOWLEDGMENTS

I would like to thank my primary advisor, Dr. Nandika D'Souza for her guidance. I have been highly benefited by her depth of knowledge and persistence while working on my thesis.

I also wish to thank Dr. Jo Ann Ratto (U.S. Army soldier Systems Center, Natick) for providing the financial support.

My thanks go to all the faculty members of Material Science Department who have been very supportive throughout my course of study. I would like to thank Dr. Robert Renka from Computer Science Department, UNT for his assistance on the MatLab programming.

I would like to thank all the group members in Polymer Mechanical and Rheology Laboratory for their co-operation. Especially, I would like to mention Laxmi Sahu for her help.

Last but not least, I am indebted for the unconditional support and encouragement provided by my family members and friends.

TABLE OF CONTENTS

Page

LIST OF TABLES

Page

LIST OF ILLUSTRATIONS

Page

CHAPTER 1

INTRODUCTION:
POLY (ETHYLENE TEREPHTHALATE) (PET) NANOCOMPOSITES

Nanocomposites based on polymer-clay mixtures are a growing area of interest due to their potential in flexible packaging applications. Improved mechanical, barrier properties and heat distortion temperature have been obtained. Most of these improvements have been attributed to the dispersion of the clay in the polymer. However as in most heterogeneous semicrystalline polymers matrix modification needs to be considered. Here we investigate the crystallization changes and dispersion of treated MLS in polymers (chapter 2). The influence of all three on the fracture mechanism is also investigated (chapter 3)

In this chapter, an introduction to heterogeneous polymers is given (section 1.1). The area of nanocomposites and terms referred to in the thesis is reviewed in consequent section 1.2 in details. And the properties of host polymer are discussed in section 1.3 followed by a plan of study.

1.1 Filler Modified Nanocomposites

Polymers are often modified by fillers to increase the modulus and decrease thermal expansivity. Particle modified polymers have been compounded with inorganic fillers like glass fibers, talc, calcium carbonate etc where the filler percentages can be as large as 60% of filler (1). The resulting composite has disadvantages such as an increase in specific gravity. Debonding between filler-polymer matrix surface due to lack of adhesion is also another problem. The tensile strength of these composites has been

studied in considerable details. If uniform strength, F_f is assumed in all the fibers, then the strength of the resulting composite is given as:

$$F_L = F_f v_f + F_m v_m \tag{1.1}$$

Where F_L is longitudinal strength of the composite, F_m is the strength of the matrix, v_f and v_m are the volume fractions of the fibers (reinforcement) and matrix respectively. Since the strength of the polymer matrix is generally much lower than the strength of the matrix the equation reduces to:

$$F_L = F_f v_f \tag{1.2}$$

From this equation one can observe that the volume fraction of the fibers has to be fairly high. This assumption of neglecting the matrix strength holds true and the composite exhibits strength according to equation (1.2) only if the fracture is fiber controlled, which may not be always the case. Incorporation of filler in significant amounts, gives rise to a number of problems. In particular, the high viscosity of the mixture results in poor processability. Further, the high specific gravity of the filler will cause a high specific gravity of a mineral filled polymer.

Another disadvantage arises due to the orientation of the filler especially when continuous fiber is used. The tensile strength of the unidirectional composite in the transverse direction is lower than the strength of the parent resin. A statement that summarizes continuous fiber composite bears thought (1), “it is easy to stiffen a reinforced plastic but difficult to strengthen it.” Introduction of nanosized fillers has produced effective way in overcoming some of the disadvantages associated with conventional composites (2, 3, 4, 5).

1.2 Nanocomposites and Their Advantages

1.2.1 Definition: Nanocomposites

Nanocomposites contain nanoparticles which have at least one characteristic length scale that is in the order of nanometers. The reinforcement can range from isotropic to highly anisotropic needle or sheet like elements. Uniform dispersion of these nanoscopic sized particles can lead to an increase in the interfacial area between the constituents. The surface area is as high as 750 to 800 m^2/g (6). This large surface area is where nanoclays are considered unique compared to conventional fillers.

1.2.2 Morphology of Nanoparticles

There are different types of natural or synthetically produced clay minerals. They include layered polysilicates, kaolinite and layered double hydroxides. Naturally occurring clay called montmorillonite, which belongs to smectite family, is most commonly used. Naturally occurring smectites are flat sheet shaped and are irregular in size. Owing to their dimensions, they have a large surface area of 750 to 800 m^2/g. They often behave as colloidal particles. This helps to keep the particles in suspension by Brownian motion. The layered silicates are further divided as smectites and silicic acid. Among these, smectites are the most widely used layered silicates and we will discuss its structure as a representative. The montmorillonite platelets are a magnesium aluminum silicate where octahedral alumina sheets are layered between two tetrahedral silica sheets (7). Within the alumina sheets replacement of aluminum cation (Al^{+3}) by magnesium cation (Mg^{+2}) results in a net negative charge to the layers. The negative charge is

balanced by hydrated inorganic cations positioned in the spacings (galleries) between the aluminosilicate layers. The gallery height is determined by the type of cation and degree of hydration. The thickness of the individual layer is around 1nm and end to end distance is 100-1000nm. This results in an aspect ratio of 1000:1

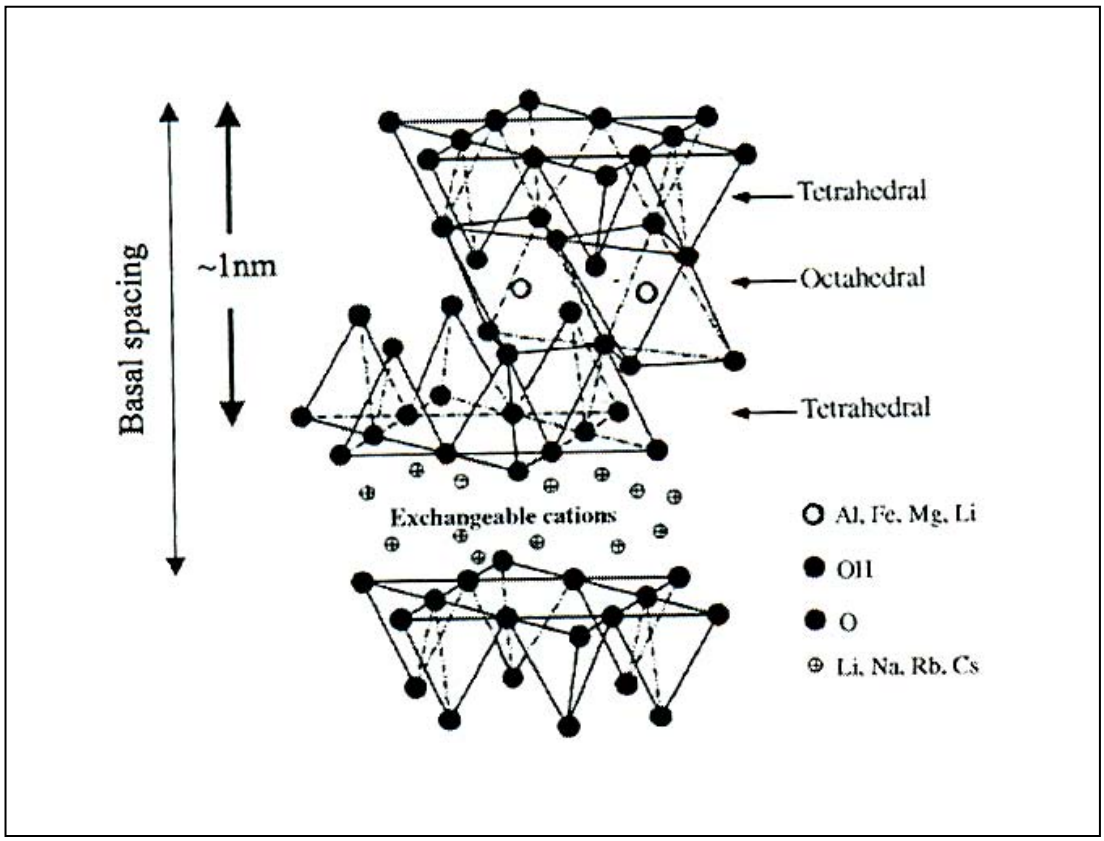

FIGURE 1.1 Structure of clays.

The clays being hydrophilic need to be modified to improve polymer compatibility. Some polymers like polyethylene oxide and poly (vinylpyrolidone) possess sufficient polarity therefore the clays need not be treated when incorporated into these polymers. Cation exchange process is followed. Inorganic cations like Ca^{+2}, K^{+} and Na^{+} are replaced by organically modified cations such as alkyl ammonium groups ($R\text{-}NH_3^{+}$).

R stands for aliphatic group. The cationic head of the aliphatic group is found close to the surface layer due to the presence of negative charges on the layer. The tail is found away from layer.

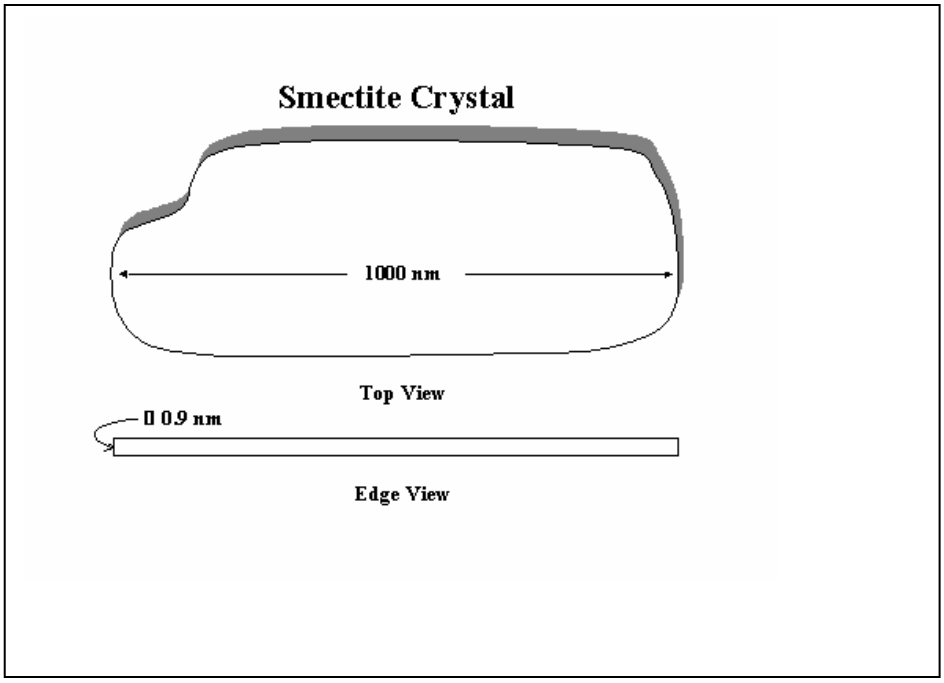

FIGURE 1.2 Schematic representation of smectite crystal. (8)

1.2.3 Type of Dispersion

The dispersion of clays depends on factors such as packing density, chain length of the organic cations, charge on the layer and processing conditions like temperature, shear, and type of bonding at the polymer-silicate surface (the type of interaction).

Depending on the type of dispersion, composite morphologies such as macrocomposite, exfoliated and intercalated dispersion are obtained. Fully exfoliated nanocomposites consist of individual nanometer thick silicate layers randomly suspended in the polymer matrix. The distance between the nanoelements begins to approach

molecular dimensions at extremely low loadings of the nanoparticles. As the dimensions of the agglomerate (also called tactoids) approach the fundamental length scale of a physical property new mechanical, optical and electrical properties arise in the resulting system. Properties absent in macroscopic counterpart are obtained. Most chains reside near an inorganic surface. Since the interphase limits the conformations that the polymer molecule can undergo, the free energy of the polymer in this interfacial region is fundamentally different from the polymer present in the bulk state. Hence only with a few volume percentages of clay, the polymer may be considered as a nanoscopically confined interfacial polymer.

In contrast to this, intercalated structures result from polymer chains residing in the silicate galleries and expansion of the original silicate layer crystallites to thermodynamically defined equilibrium spacing (also called as swelling the clay layers). The primary particles (crystallites or tactoids) consist of well-ordered alternating polymer/ silicate layers with a repeat distance of few nanometers. These have been utilized as a model system to study the dynamics of ultra confined polymer layers.

In practice many systems do not follow these idealized polymer morphologies because fabrication of nanocomposites involves physical mixing of the polymer (or monomer) with micron scale agglomerates comprised of hundreds of crystallites and hence thousands of layers. Hence intermediate states or mixed morphologies are more common. They arise from inhomogeneities in size and composition in natural smectites, processing factors or kinetic aspects associated with translational mobility of large aspect ratio plates in a viscoelastic medium. The highest property enhancement is associated

with true exfoliated morphologies. The intermediate morphologies too provide certain improvements in the properties based on the presence of the nanoscopic, high aspect ratio particles (which consist of individual layers and aggregates containing 3-5 layers). In practice, polymer nanocomposites, whether thermodynamically stable or metastable, are comprised of hierarchical structures with primary features associated with individual layers and secondary features associated with arrangement of individual layers or stacks of layers.

1.2.4 Method of Preparation

1.2.4.1 In Situ Polymerization

The ion exchanged layered clay is mixed with the monomer. In the presence of clay, the monomer is polymerized. The first commercial nanocomposite developed by Toyota was by this method for Nylon 6. The properties of these nanocomposites were substantially improved. Nanocomposites from polymers such as polyacrylates, methacrylates, polystyrene, SBR, epoxy, polyester and polyurethane can be used in the in situ polymerization approach. There are many polymers which can not be used in this method e.g. polyolefins.

In polyesters like PET, the polymerization process is a 2 step mechanism. Hence there are some difficulties in the polymerization process and debate over the step in which the clay should be added. As the polymerization process advances, the molecular weight increases and consequently polarity decreases. Higher polarity is associated with an exfoliated structure. Hence as the molecular weight increases in polyester, the phase

separation of polymer and the clays occurs. Hence clay treatment is necessary in this case.

1.2.4.2 Melt Intercalation Process

This commercial process of nanocomposite preparation was investigated by Gianellis (7). This method involves preparation of nanocomposites via direct compounding of polymer with the clays. Comparison of the properties of the nanocomposites prepared by in situ polymerization and melt blending shows that the degree of exfoliation with in situ polymerization is slightly greater than the melt intercalation process. The physical properties can also be correlated well with the dispersion. But this small improvement in properties is balanced against the potentially lower cost of the melt intercalation process. For polyolefins, this is the only possible route of preparation of nanocomposites.

1.2.4.3 Polymer Solution Intercalation

Here, the polymer is dissolved in a suitable solvent, in which the silicate layers can be swellable. The clay is mixed with the solvated polymer and then the solvent is removed. This method is suitable for laboratory scaled experiments, and is of little commercial importance.

1.2.5 Characterization Techniques

Traditionally, observation and detailed characterization of polymer nanocomposite morphology has been done mostly based on techniques like wide angle x-ray diffraction in reflection geometry (WAXD) and transmission electron microscopy (TEM). WAXD is useful in rapid characterization. But it is limited in resolution (<6nm) and is very sensitive to surface alignment and preparation procedures at very low diffraction angles ($1^o < 2\theta < 5^o$), which are necessary for characterization of layered silicates. TEM on the other hand, has very high resolution power, but it essentially represents a very small cross section area of sample. The typical dark lines present in the TEM micrograph of a nanocomposite represent the edges of the individual silicate layers.

1.2.6 Advantages of Polymer Nanocomposites (9)

With polymer nanocomposites, desired properties can be achieved with the help of very low clay loadings of less than 5 wt%. In automotive applications, this weight saving directly transfers to fuel economy. Nanocomposites provide efficient reinforcement without significant loss of ductility or impact strength. Their thermal endurance and flame resistance is exceptional as they form a char layer preventing further burning in case of fire. They have improved barrier properties. Apart from this, improved abrasion resistance, reduced shrinkage and residual stress are some of the other advantages. They can be easily extruded or molded to near final shape. At the same time they have altered electrical, electronic and optical properties.

1.2.7 Applications of Nanocomposites

Typical applications include automotive under the hood applications where high heat distortion temperature is a prime requirement. Commercial use has been in the timing chain cover for Toyota. Carbon nanotubes, which have the capability of imparting conductivity to the polymer matrix, improve the electrostatic paintability and are used commercially in PPO/PA blend by GE plastics.

Other potential uses are in barrier applications. There have been 2 mechanisms suggested for alteration of the permeability behavior in nanocomposites. The first one is development of a tortuous path of the diffusing molecule and second one is large interfacial volume of the nanocomposite. The tortuous path mechanism considers the clay particle as a non permeable entity and in a nanocomposite; the diffusing species has a repeatedly altered vector and hence much longer diffusion pathlength. The second one, the large interfacial volume mechanism contends that the larger surface area of exfoliated clays causes most of the host polymer to lie close to the clay-polymer interface which in turn restricts the mobility of the polymer molecules and any molecules attempting to diffuse through the polymer. Improved barrier properties may be by both these mechanisms. This leads to replacement of multilayer packaging material by these polymer nanocomposites. Commercial grades of Nylon 6 for packaging films are available from Ube and Bayer.

The use of nanoclays in flexible packaging market is investigated widely (10). Properties required by an efficient packaging material like hot fill, moisture barrier, thermoforming were obtained in nanocomposites. However this application is still in the

very initial stage and there are still some challenges to be fulfilled e.g. gaining FDA approval, investigate base polymers other than polyolefins, study the effect of film orientation in blown, cast nanocomposite film etc. Commercial applications in flexible packaging are being developed in this area and first commercialized nano film is expected to be introduced in 2005.

1.3 Poly (ethylene terephthalate) (PET): Characteristic Properties

Polyesters are heterochain macromolecular substances characterized by the presence of carboxylate ester groups in the repeating unit of their main chain. Poly (ethylene terephthalate) (PET) is a commercially used terephthalate polyester with a general chemical structure as follows

$$-\left(O\left(CH_2\ \right)_x O-C O-(C_6 H_5)-CO-\ \right)_n$$

Where x is 2 or 4

1.3.1 Development and Application (11)

PET was invented in United Kingdom during early years of world war II. It was recognized as a fiber forming polymer, and manufacture and commercial development started in 1950's by ICI Ltd in UK and by Du Pont in the US. The trade names introduced by these companies were Terylene and Dacron respectively. The trade names in film manufacturing are Mylar, Melinex etc.

PET has typical applications ranging from fibers, films and blow molded bottles. The fibers are used in various industrial applications like sewing threads, tire cords, filter

fabrics. Blends of PET-wool-celluloisic fibers are used in apparel, curtains, upholstery, fiberfill applications. PET films have a wide variety of applications in packaging of metallized and printable forms, laminated form for food packaging like coffee, boil in a bag applications etc. to medical and surgical device packaging due to temperature stability during sterilization and clarity. The applications based on electronic industry include bases for magnetic, video and computer tapes, electrical insulation and membrane switches displays, pressure sensitive tapes, photoresist. The other film applications mainly consist of photographic and drafting films, hot stamping foils, fiberglass reinforced panels, ID and smart cards. Bottles are popular for use in carbonated soft drinks, wines, beers, spirits as well as miscellaneous industrial liquid products.

PET has excellent thermal, moisture and chemical resistance. It can withstand temperatures ranging from -70^{o}C to 150^{o}C making it suitable to use in extended drying ovens, hot stamping etc. PET has low moisture absorption at room temperature. PET shows moisture absorption of 0.4% at the relative humidity of 63% and room temperature with less than 1% shrinkage in boiling water. It is resistant to dilute aqueous mineral acids, nonbasic salts and many common organic compounds. Its barrier properties are exceptional, particularly in case of number average molecular weight of more than 26,000. Flavor preservation is key factor in food packaging and the barrier properties of polyesters are second to aluminum foil. Polyester film retains flavor and excluded odor from outside (12). It is inherently more recyclable than other plastics and has capacity to include recycled content.

It is prone to attack by oxidizing reagents, particularly by aqueous alkalies, ammonia and lower amines. At high temperature, under humid conditions, the ester group is hydrolyzed to OH and COOH group, especially above 150^{o}C, the hydrolysis is rapid. Hence PET must be dried to retain moisture content of not more than 30ppm.

1.4 Plan of Study

Nano sized clay platelets can significantly alter the morphology of polymer matrix, especially when the polymer under consideration is semicrystalline. The effect of incorporation of montmorillonite layered silicate (MLS) on the crystallization of poly (ethylene terephthalate) (PET) will be investigated. Non isothermal as well as isothermal crystallization kinetics is studied with the help of differential scanning calorimeter (DSC), polarized optical microscopy (POM). The thermal analysis data is further studied with Avrami analysis. The effect of matrix modification is correlated with the mechanical properties, toughening mechanism in particular using essential work of fracture approach with the aid of mechanical testing system, infrared thermography.

1.5 References

[1] Mark, Bikales, Overberger and menges, Encyclopedia of Polymer Science and Engineering, **3**, 776 (1985).

[2] A. Hernandez-Luna and N. D'Souza, ANTEC, 1461 (2002).

[3] A. Ranade, N. DSouza and B. Gnade, Polymer, **43**, 3759(2002).

[4] W. Strauss and N. DSouza, J of Cell. Plastics, **40**, 229 (2004).

[5] A.Ranade, N.D'Souza,B. Gnade and A. Dharia, J of Plastic films, **19**, 271(2003).

[6] K. Kamena, Polyolefins, Houston (2005).

[7] T. Pinnavaia and G. Beall, Polymer-Clay nanocomposites, Wiley Series, 233(2000).

[8] Figure reproduced with permission from Southern Clay Products, Inc. www.scprod.com

[9] J. Collister, Polymer Nanocomposites, ACS symposium series 804, 7.

[10] V. Zabrocki, Flexible Packaging Conference, 2005.

[11] Mark, Bikales, Overberger and Menges, *Encyclopedia of Polymer Science and Engineering*, **12**,19(1985).

[12] A. Brody and K. Marsh, *Encyclopedia of Packaging Technology*, Wiley (1997).

CHAPTER 2

POLY (ETHYLENE TEREPHTHALATE) (PET) NANOCOMPOSITES: EFFECT OF NANOCLAY ON CRYSTALLIZATION

2.1 Introduction

Crystallization in polymers is a complicated phenomena influenced by a number of factors such as the flexibility of the repeating unit, symmetry of side chains and presence of heterogeneous particles. As a consequence, the geometry of the crystal formed varies over a wide range. The size of crystallites, their distribution and uniformity determine the mechanical, optical and overall properties.

Crystallization from melt is feasible when the Gibb's free energy is negative.

$$\Delta G = G_{crystal} - G_{melt} \tag{2.1}$$

$$\Delta G = \Delta H - T\Delta S \tag{2.2}$$

A crystal has a small size in the beginning and hence very large surface area. The overall free enthalpy of crystallization (Δh_c) is higher and for a surface area of A and free energy γ, the free enthalpy of crystallization is represented as

$$\Delta G = \Delta G_c + \sum \gamma A \tag{2.3}$$

The initial process leading the crystal from the amorphous state when the free enthalpy of crystallization is the highest is termed as primary nucleation. Before a nucleus of critical size is developed, the primary nucleus is created when ΔG is positive. The critical size of nucleus is attained when ΔG is the maximum. Nuclei to the left are

called subcritical nuclei and to right of this maximum are the supercritical nuclei. Nuclei with negative ΔG are called stable nuclei or small crystals.

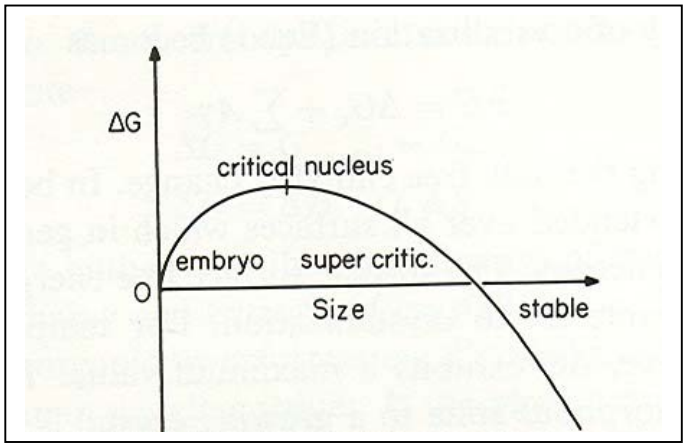

FIGURE 2.1 Schematic representation of nucleation as function of free enthalpy of crystallization (1).

Homogenous nucleation refers to nucleation in the absence of a foreign substance. If the homogenous crystallization occurs due to the crystals, which have similar chemical structure as the parent polymer and have remained after the melting of the crystal, it is called athermal or self nucleation. On the other hand, if a foreign surface acts as the nuclei, it is termed as heterogeneous nucleation.

The evolution of crystallinity can be explained with the help of various mathematical models like Avrami, Tobin, Ozawa, Kolmogroff-Avrami-Evans models etc. Avrami analysis is an effective way to find out crystallite geometry confined to 3 dimensions.

2.1.1 Avrami Model

The Avrami model gives a mathematical representation of crystallite formation on a macroscopic level. The Avrami equation was developed using the analogy of waves created by raindrops falling on a pond. Each raindrop makes a circular wave front and the probability of such wave fronts meeting a representative point P with respect to time t is calculated. In a similar basis, the Avrami equation and parameters are derived considering the probability of a number of spherulites impinging on each other at point P at time t [2]. It is stated as,

$$X(t) = 1 - \exp[-(Kt^n)] \tag{2.4}$$

Where X (t) is relative crystallinity at time t., K is crystallization rate constant. n is Avrami exponent.

From equation (2.4) we have,

$$\ln\{-\ln[1 - X(t)]\} = \ln K + n \ln t \tag{2.5}$$

Slope of the graph $\ln\{-\ln[1 - X(t)]\}$ against $\ln t$, gives n (Avrami exponent) and intercept gives crystallization rate constant K. The Avrami exponent n corresponds to the dimensionality of the crystallite and K indicates concentration of nuclei. For the case of athermal nucleation crystallite shape will be linear if n is equal to 1, circular if n is equal to 2 and spherical if n is equal to 3. Intermediate values of Avrami correspond to different crystallite shapes like ribbon or fibrillar (≤1), circular, lamellar (≤2). An Avrami exponent of 2 to 4 was observed during PET nucleation where 2 indicates that crystals formed were the chain folded crystals (2). Lu et al. (3) studied the isothermal crystallization kinetics and melting behavior of PET using the differential scanning

calorimetry (DSC), the data was analyzed by the Avrami equation. The Avrami analysis indicated that the primary crystallization of PET followed the mechanism of three-dimensional spherical growth on heterogeneous nuclei and secondary nucleation was linear growth formed within the spherulites.

2.1.2 Crystallization in PET

The PET crystal has packing similar to polyethylene. Repeating units of odd numbers of chain atoms crystallize in an orthorhombic system and even number of atoms in a monoclinic system (4). From the figure (2.2) it can be seen that the ester groups are tilted about 12^{o} out of plane of the benzene rings.

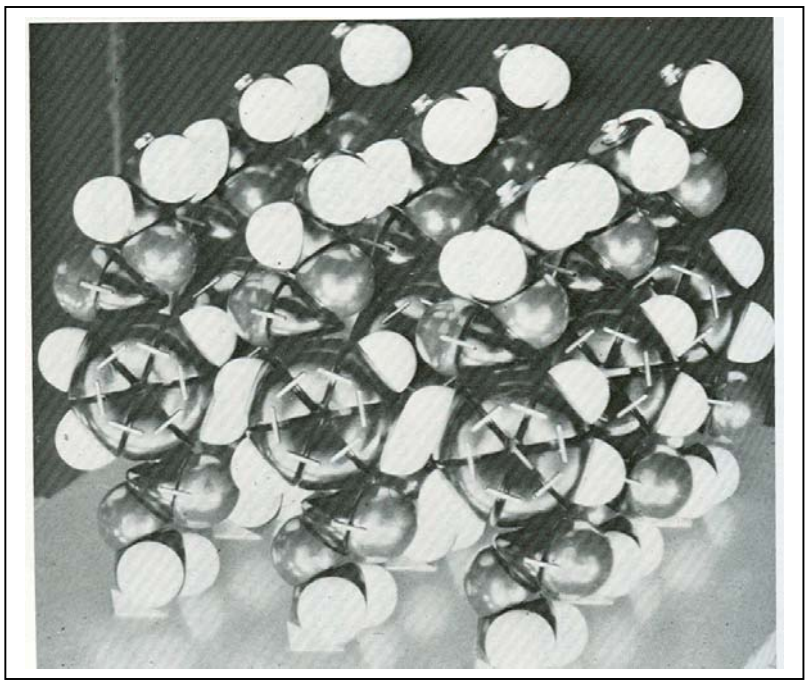

FIGURE 2.2 Model of the triclinic PET crystal structure (5).

Lower crystallization rate and low degree of crystallinity are characteristics of PET. Crystallization rates of PET, which has 2 methylene groups) was found to be lowest compared to other polyesters like poly (trimethylene terephthalate) (PTT) and poly (butylenes terephthalate) (PBT) which have 3 and 4 methylene group respectively (6). Dixon et al. (9) have reported degree of crystallinity in the range of 57% to 61% for a PET having an intrinsic viscosity in the range of 0.65 to 1.28. They also observed that spherulitic size of pure PET in the range of 20 to 50 microns, which decreased to 1 to 10 microns on addition of 0.5 wt% of talc.

Crystallization in PET depends on a number of factors like molecular weight (represented by intrinsic viscosity), thermal history, the nature of the polymerization catalyst used, presence of nucleating agents and copolymer units (7), (8). The crystallization in PET is temperature dependent. The maximum rate of crystallization is found in the range of 150^{o}C to 180^{o}C. Crystallization can be either controlled by heat diffusion and by surface kinetics on rough interface or by nucleation controlled kinetics of melting. Toda et al. (9) determined that nucleation controlled kinetics affect melting in PET.

PET also has a tendency to undergo reorganization by fold opening and stress removal by re-polymerization to undergo crystal perfection. At sufficiently high temperatures and conditions, trans-esterification occurs below the melting point. This process takes place in amorphous regions and stress caused by initial crystallization and subsequent deformation can be removed and chain folds can be opened. Re-

crystallization in polymers is in general a fast process and it is difficult to prevent re-crystallization on heating to partial melting temperatures at normal heating rates (10).

2.1.3 PET Crystallinity: Effect of Processing Parameters

A crystallization study in PET is of special importance considering the range of processing post processing applications it undergoes. Isothermal crystallization, for example, is encountered in typical PET processing methods like reheated stretch blow molding of bottles, heat setting and production of films and fibers (11).

The effect of heat setting treatments on the crystallinity was studied in oriented non crystalline PET fibers in terms of parameters like thermal shrinkage and elongation with the help of X-Ray diffraction and FTIR spectroscopy (12). A mesophase structure was noted in these fibers, i.e. chain extended non crystalline phase. The amount of thermal shrinkage was less in the fibers having a mesophase compared to the completely amorphous fibers, which are non oriented and non crystalline.

The effect of annealing temperature on the crystallization phase was studied (13). Annealing PET at 270^{o}C for 472.5 hours yielded a crystalline phase stable to 10^{o}C higher than the equilibrium melting point without loss of structure of PET. This high melting point suggested that the crystals possess a substantial extended chain structure.

2.1.4 Strain Induced Crystallization in PET

Semicrystalline fibers and films of PET are produced by applying strains above the glass transition region. This stretching process generates molecular orientation, which results in strain induced crystallization.

Since PET shows strain induced crystallization on orientation, the effect of biaxial stretching on crystallinity has been studied by Chandran and Jabarin (14). They found the changes in crystallinity in terms of density changes. Interestingly they observed that samples stretched in sequential mode showed higher crystallinity, with evidence of strain induced crystallization, than those stretched in a simultaneous mode where no strain induced crystallization occurred.

Crystallization kinetics of previously oriented PET sheets was studied under isothermal and nonisothermal crystallization conditions (15). As the stretch ratio increases, the rate of crystallization increased with subsequent decrease in activation energy for crystallization. Similarly the effect of orientation on crystallinity was studied (16), (17), (18)

An interesting effect of TiO_2 particles on the crystallization of the PET matrix was found during deformation by Taniguchi et al. (19). TiO_2 was found to have a nucleating effect on the PET matrix (20). Addition of submicron sized TiO_2; however, had a denucleating effect during deformation of PET. This suppressed the mechanical relaxation process and reduced strain hardening and subsequent strain induced crystallization. This effect was attributed to the reduction in chain entanglement in the

PET matrix due to high surface interactions between the filler particles and the PET matrix.

2.1.5 Thermal Transition in PET and Effect of Crystallinity

PET is a semicrystalline polymer and has thermal transition such as T_g, cold crystallization and dual melting peaks. Hence it is interesting to consider the thermal transitions taking place in case of PET and the effect of change in crystallinity on these transitions in relation to different processing parameters.

The melting peak in a polymer gives useful qualitative information about the size of the spherulites and their size distribution. Hence ultimately, it gives the degree of crystallinity present in the polymeric sample. PET often has multiple endothermic transitions as the material approaches melting. The melting temperature is approximately 290^{o}C.

Cold crystallization peak (or peaks) is observed in PET when the sample is heated. Effects of annealing have been studied on the cold crystallization behavior of PET. Polymer matrices are constituted of crystalline lamellae separated by amorphous phases. The crystalline lamellae consist of polymeric chains. When the crystallization process is hindered, the growth of spherulites is not complete leaving the interspherulitic region more amorphous than interlamellar region. Hence crystallization from interlamellar amorphous regions is easier and this region undergoes crystallization. This is called cold crystallization temperature. The interspherulitic region also undergoes cold

crystallization. At a higher temperature compared to cold crystallization due to ineterlamellar region.

2.1.6 Effect of Heterogeneous Particles on the Crystallization

So far we have mostly dealt with the effects of crystallinity in case of pure PET. The addition of heterogeneous organic filler in a semicrystalline polymer matrix can yield altered matrix properties due to the nucleating effect the filler can have on the system. The effect of this filler in terms of dimension of the filler particle, compatibilizer used (21) and treatment of the filler (22) was studied by various authors.

The degree of crystallinity achieved in PET was found independent of the type of filler (23). The effect of fiber reinforcement on crystallization was studied with glass and Kevlar fibers. From optical microscopy observations they found that the glass matrix had less nucleating ability than Kevlar fiber. Additionally, the plasticized PET had greater crystallization rate compared to pure PET due to enhanced mobility of the system.

Cheng et al. carried out isothermal DSC followed by Avrami analysis to compare the crystallinity obtained by various fillers in a PET matrix. Athermal nucleation was inhibited by the presence of fillers. Mobility of polymers in the melt was reduced due to the presence of these fillers. As the filler changed from carbon, titanium dioxide, glass fiber and calcium carbonate, a decreased crystallization temperature, decreased crystallization half times, increased activation energy was observed (24).

The effect of talc, kaolin, silicon dioxide and titanium dioxide on crystallization of PET was found to vary with concentration (0.2-0.3 vol. %), size distribution and

nucleating ability of the nucleating agent (25). Talc and titanium dioxide were the most effective.

A copolymer unit also acts as a heterogeneity affecting the crystallinity in the polymers. The effect of hydroquinone on crystallization of PET was studied by Sakaguchi with the hydroquinone content of 2-11 mol% (26). 2 mol% of hydroquinone showed decreased crystallization rate whereas 6 and 8mol% of the copolymer unit showed higher nucleation rate. 11mol% copolymer unit showed crystallization rates thrice as high as the pure PET. An opposite effect was found on the crystallization kinetics of PET in presence of ethylene isophthalate unit (27). The copolymer unit was found to hinder the crystallization of PET.

2.1.7 Nanocomposites and Crystallization

Polymer nanocomposites pertain to a special case of such heterogeneous organic filler where due to nano scale dimensions, a more pronounced effect on crystallization is observed. Liu et al. (28) and Ranade et al. (29) have shown that in the presence of MLS platelets, nylon crystallizes in the γ form instead of the usual and more stable α form. Hence corresponding to the γ form, the properties of the nylon nanocomposite can be predicted. For syndiotactic polystyrene, the presence of MLS was found to have a favorable effect on the crystallization, in the sense that thermodynamically favored trans β crystallites are formed (30). The PS nanocomposite was prepared by solution intercalation process. The addition of MLS helped overcome the energy barrier of chain conformation transformation facilitating gauche to trans transformation. Highest

crystallinity was obtained in the nanocomposite where the β crystal is formed. Therefore it was concluded that MLS significantly affected both the conformation and crystallinity in syndiotactic PS crystallite. Hence insight in the crystallization behavior of polymer nanocomposite can be utilized in order to model their service performance. Sheng et al. (31) have predicted the mechanical properties of semicrystalline Nylon 6 polymer nanocomposite by the simulation of the polymer matrix in three distinct phases viz. nanoparticle, crystallized anisotropic matrix, and isotropic matrix.

The first nanocomposites were prepared by the Toyota group utilizing nylon-6 and MLS in an in-situ polymerization process (32), (33). They observed a cationic interaction between the polymer matrix and MLS platelets along with a decrease in molecular weight on increasing the MLS content. This indicated interaction between the polymer matrix and the MLS platelets. Consequently, they found that the crystallinity in the nanocomposite was lower than that of pure nylon6 (34). The orientation of nylon 6 crystallite in nanocomposites was different than pure nylon. They did not observe any changes in crystal form. Despite this, they observed large increases in tensile strength in the polymer nanocomposite.

2.1.8 Presence of Nanoclay: Hindrance to Nucleation or Reduced Crystallization

Hindered nucleation in nanocomposite has also been determined in some systems. Krikorian et al. (35) found reduced crystallization in poly (L-lactic acid) - MLS system compared to the pure PLA with exfoliated morphology showing lower crystallinity compared to the intercalated one. Two types of MLS-with varying degree of

organophilicity were used in this study. Nanocomposites were prepared by solution intercalation method followed by film casting. The nanocomposite with more organophilic MLS resulted in exfoliated structure while that with less organophilic MLS resulted in an intercalated one. The exfoliated morphology also yielded bigger spherulites owing to increased spherulitic growth rate in the presence of MLS. Interestingly, the reduced nucleating ability of MLS in an exfoliated structure was attributed to miscibility between MLS with polymer. Hence it was found that more organophilic MLS is not an effective nucleating agent in comparison with the other type of MLS due to higher compatibility of organophilic MLS with PLLA. In this case, the fully dispersed clay platelets acted as a template for spherulitic growth which resulted in much larger spherulites. Despite this, the overall crystallinity in PLLA-organophilic MLS was lower compared to neat PLLA or PLLA and less organophilic MLS. Hence organophilic MLS was said to hinder the local crystallization and hence the ultimate bulk crystallization was hampered. The exact mechanism of templating is under investigation. Fornes et al. (36) have found that the crystallinity of nylon6 matrix increases on addition of MLS only upto 1.6 wt% of MLS, after which the crystallinity of the matrix decreases. They found a skin core effect in the injection molded nylon nanocomposite samples. The outer or skin layer of molded specimen was found to contain only γ crystals while the core contained both γ and α form of crystals. Higher crystallinity was observed in the skin rather than in the core in the nanocomposite and vice-a versa in case of pure nylon moldings. Limitation in chain mobility is associated with formation of γ crystals. Hence addition of clay platelets decreased the mobility of chains in the polymer nanocomposite

system leading to increased possibility of γ crystal formation. Similar results were obtained by Jimenez et al. (37) in case of poly (ε-caprolactone)-MLS system. Weng et al. (38) found increased activation energies and decreased melting point in nylon/exfoliated graphite nanocomposite. The nanocomposites were prepared by in situ polymerization. The equilibrium melting temperature obtained is lower in nanocomposites as compared to the pure polymer.

The effect of MLS on spherulitic growth was also studied. Wan et al. (39) have reported the presence of three dimensional irregular shaped crystallites in PET nanocomposites which were smaller than neat PET. The PET-3%MLS nanocomposites were prepared via in situ polymerization. A partially exfoliated morphology was obtained in the PET nanocomposites with the extent of exfoliation being low. They found increased rate constants by Avrami analysis, but predicted the presence of defects in crystalline region of PET nanocomposite by FTIR technique. The crystal growth was also found to be terminated due to the presence of MLS platelets. The crystallites were found to be irregularly shaped and interlocked with each other. The polymer chains near the MLS platelets got tethered to the platelets leading to strong interaction between the two and hence the crystallites got terminated on MLS platelets. Similar results were obtained by Lincoln et al. (40) in nylon crystallites. They emphasized the importance of mesoscale (secondary) structure arising from MLS and its impact on crystallite morphology. Smaller, more disordered lamellae were obtained in in-situ polymerized nanocomposites whereas larger, more ordered lamellae were obtained in melt –processed nanocomposites. The in situ polymerized nanocomposite had this crystallite structure as the polymer

chains were attached to silicate surface which reduces the chain mobility. Reduced mobility led to smaller, less ordered crystallites. While in melt processed nanocomposite, polymer chains weakly interacting with silicate layer were not impeded and were easier to incorporate in the crystal surface. They also showed that the interfacial area between the polymer and silicate layer had an effect on the short range order of the crystallites. Despite the occurrence of disordered crystallites in nanocomposites, the extent of crystallinity was higher on addition of silicate.

2.1.9 PET Nanocomposites

PET nanocomposites are not studied in great details as compared to nylon and polyolefin nanocomposites. This can be generally attributed to the fact that the enhancement in properties in PET nanocomposites is not as noticeable as in the above mentioned polymers. Ke et al. (41) prepared PET-MLS nanocomposites by in-situ polymerization process. They used MLS content of 0.5, 1, 2, 3 and 5%. It was seen that the melting temperature decreased on addition of MLS, with 5% PET nanocomposite showing a maximum melting temperature drop of 7^{o}C. At the same time they observed a constant increase in weight average molecular weight and number average molecular weight on incorporation of MLS, with consequent decrease in polydispersity index showing that more unbranched structure was obtained in PET on addition of MLS. Avrami analysis carried out from the isothermal crystallization proved that there is a change in crystallization behavior after MLS addition of 2.2 wt % which indicates that MLS created heterogeneous metastable or unstable lamellae state in the PET

nanocomposite. The splitting of the diffraction peak also supported these results. Overall they found increase in crystallization rate on addition of MLS. At the same time the hindering effect of MLS was found in terms of finer crystallites resulting in better optical properties. They have also studied effect of different clay reagents on the morphology.

PET-MLS nanocomposite system prepared by in situ polymerization was investigated for the crystallization effects. An increase in intrinsic viscosity was obtained in PET nanocomposite than pure polymer. The intrinsic viscosity of pure PET was 0.56 whereas for PET -5%MLS nanocomposite system, it was 0.68. They have reported 3 times greater crystallization rate measured in terms of time of crystallization in non isothermal crystallization in PET-MLS nanocomposite compared to pure PET (42). But their data showed retardation in melting point on addition on MLS. Ou et al. (43) have found that Na-MLS acted as a nucleating agent in PET matrix in terms of reduced time of crystallization and subsequent increase in enthalpy of crystallization on addition of Na MLS. Na-MLS is the naturally occurring MLS without any pretreatment. The nanocomposite was prepared by solution intercalation with MLS loading of 1 to 15wt % and reported enhanced crystallization at PET/10%MLS. Similarly Sanchez et al. (44) investigated PET-MLS system along with two compatibilizers i.e. pentaerythrytol and maleic unhydride. The blends were made by melt processing method. They found that the crystallinity increased along with the modulus and strength in the presence of compatibilizers. This enhancement in crystallinity is found especially at low concentrations of MLS. They found that PET-MLS nanocomposites without any compatibilizer showed decreased crystallization temperature than neat PET. Addition of

compatibilizer further decreased this crystallization temperature. At the same time there was no noticeable effect on the melting temperature. And the enthalpy of melting increased. This effect was attributed to the production procedure used by the authors. Improvements in mechanical properties were also obtained. Interestingly they also reported a decrease in shear viscosity in PET on addition of MLS. This will result better surface properties with smaller shrinkage in the mold in injection molding process and hence is beneficial. Similarly, Davis et al. (45) reported the influence of MLS treatment on the dispersion properties in case of PET. They used 2 types of modifiers for the MLS and melt blended the PET nanocomposites. The modifier which had a decomposition temperature of 250^{o}C (i.e. less than the processing temperature of PET) led to PET nanocomposites which were black, brittle and tar like. The highest exfoliation was observed with a melt blending at a certain shear rate and conditions. Alternate mixing conditions, (like higher shear rate or increased residence time) resulted in low quality nanocomposites. The physical properties were not evaluated in this article. The modifier which had decomposition temperature of 350^{o}C, which is well above the processing temperature of PET showed high levels of dispersion and delamination under processing conditions.

Hu et al. (46) have found a nucleating effect in poly (trymethylene terephthalate) (PTT) matrix on addition of MLS. The commercially supplied PTT with intrinsic viscosity of 0.92 dl/g and Na MLS nanocomposite system was used. Some other clay with different cation exchange capacities were also used namely 10A, 15A, 20A, 25A, 93A and 30 B. The hydrophilicity of these MLS types varies in following order:

30B>10A>25A>93A>20A>15A. Except Na MLS and 15A, there was an intercalated structure present for all the other MLS whereas in the Na MLS and 15A nanocomposites; there was complete absence of the peaks. XRD results showed an increase in diffraction intensity towards lower angle as hydrophilicity increases. The nucleation effect was found in all clays accompanied by an increased heat of fusion in PTT nanocomposites. This effect was pronounced at 3% MLS composition. They carried out extensive drying of both polymer as well as MLS.

In our experimental set up, we tried to simulate processing conditions encountered in practice. E.g. high quench rate non-isothermal study represents the conditions in injection molding of PET bottles and low quench rates, which reflect heat setting and many such post molding operations. It is desired that there be a nucleation delay at low quench rates in the post molding operations while at high quench rates, we need faster nucleation to occur. The objective of this study is to study the effect of MLS on the crystallization onset of semicrystalline PET and to study the role of MLS during nucleation of PET, effect on spherulitic dimensions as a function of quench rates.

2.2 Experimental

2.2.1 Materials

Extrusion grade semi-crystalline PET was supplied by KOSA. Cloisite 30B was obtained from Southern Clay. This is a natural MLS modified with alkyl quaternary ammonium salts.

2.2.2 Preparation of Nanocomposite

PET pellets were dried overnight in a desiccant drier at 80^0C. A 10% by weight master batch of clay with PET was prepared on a Thermoprism co-rotating twin-screw extruder of 16 mm screw diameter and L/D ratio of 24:1. The standard screw design with good dispersion characteristics was chosen for the master batch preparation. Individual compositions of (1, 2, 3 & 5% by weight) were prepared by mixing appropriate amounts of the master batch with neat PET.

2.2.3 X-ray Diffraction

A Siemens D500 X-ray Diffractometer was used to study the diffraction behavior of clay nanocomposites. All the experiments were carried out between 2Θ equal to 2^o to 60^o. PET nanocomposite pellets were crushed into powder by a cryo technique. Experiments were carried out at room temperature. The basal spacing or the d spacing was calculated by using Bragg's equation.

2.2.4 Differential Scanning Calorimetry (DSC)

The crystallization study was carried out on a Perkin-Elmer Pyris 6 differential scanning calorimeter (DSC), with indium calibration. The pellets of PET/MLS nanocomposite ranging in weight from 5-10mg were used for each run.

For the non-isothermal study, the sample was initially heated from 30^oC to 260^oC at a rate of 45^oC/min followed by heating at 10^oC/min and cooling at different rates, i.e. 1, 25, 40, 45 ^{o}C/min.

For the isothermal crystallization, the sample is heated from 30^0C to 280^0C at a rate of 10^oC/min and held at 280^0C to destroy any residual nuclei. Then it is cooled at appropriate crystallization temperature at rate of 50^0C and held at crystallization temperature for 10 min. The sample is further cooled from the crystallization temperature to 30^0C and 50^0C. This is to ensure that all the crystallization present in the sample can be attributed exclusively to the isothermal crystallization temperature.

2.2.5 Polarized Optical Microscopy

Optical microscopy (OM) was conducted on a Zeiss optical microscope. The lens magnification was 40X. The pictures were taken using a CONTAX camera. The pellet section was heated above the melting temperature and cooled slowly. Various stages in crystallization starting from melt state were recorded.

2.2.6 Transmission Electron Microscopy (TEM)

The TEM study was conducted on a JEOL JEM-100CX II electron microscope. A MT6000 Sorvall microtome was used to cut the thin sections of the sample.

2.3 Results and Discussion

2.3.1 Dispersion Analysis

Figure 2.3 shows the x-ray diffraction (XRD) pattern of PET nanocomposites. Organically treated MLS has two characteristic peaks at low 2Θ equal to 4.6^0 (001) and 9^0 (002). 1% and 2% PET nanocomposites show complete disruption of characteristic

peaks. The disruption of the MLS structure reflects exfoliation at 1% and 2% concentration. In polymer nanocomposites, an increase in MLS concentration shifts the level of dispersion from exfoliation to intercalation to an agglomerated system. XRD analysis of 3% and 5% PET nanocomposites (Fig2.3) showed partial disruption and shift in the characteristic (001) peak. The intensity of the peaks increased. The platelet spacing increased from 19A^{o} to around 38A^{o} (around 100%) for (001) with increase in MLS concentration.

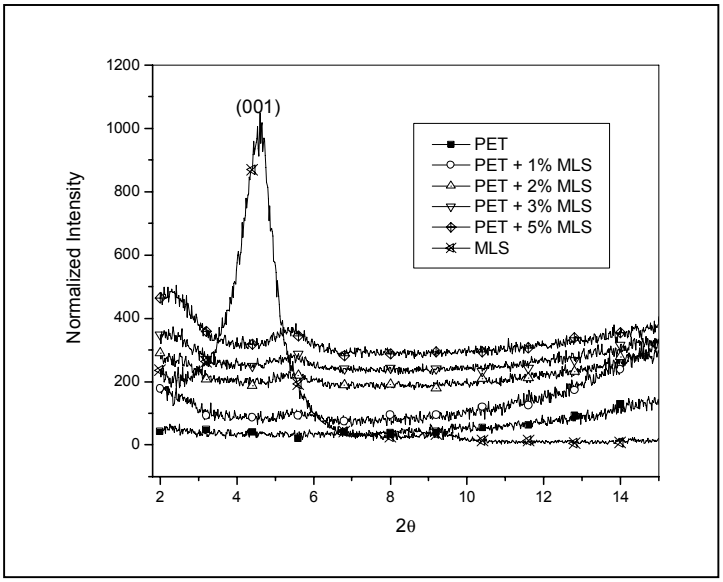

FIGURE 2.3 X-ray Diffraction patterns of PET Nanocomposites.

Figure 2.4 and 2.5 shows the TEM micrographs of 1% and 5% PET nanocomposites. The dark lines represent MLS platelets with an average thickness of 20A^{0} to 50A^{0}. The average spacing between silicate galleries is shown in Table 1. 1%, 2% and 3% PET nanocomposites showed wide average platelet spacing. TEM analysis showed the

presence of exfoliation at lower MLS concentration followed by exfoliated-intercalated structure at higher MLS concentration.

FIGURE 2.4 TEM of 1% PET Nanocomposite.

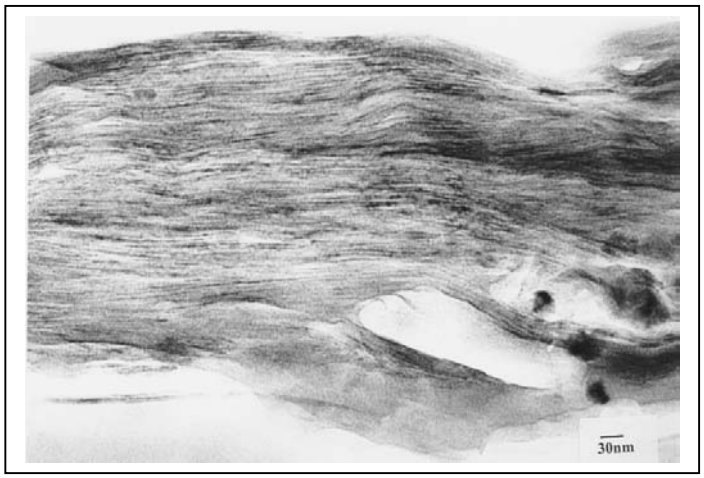

FIGURE 2.5 TEM of 5% PET Nanocomposite.

TABLE 2.1 Average spacing between observed silicate galleries during TEM analysis.

TEM Micrographs	Platelet Spacing, A^o
1%	50
2%	44
3%	40
5%	39

2.3.2 Optical Microscopy

Fig 4 shows uniformly dispersed spherulites in a polarized optical micrograph of neat PET. The change is not significant and 1% MLS had little or no effect on the crystallite dimension of PET. Continued addition of MLS (2%, 3% and 5%) showed a sharp change in the size of spherulites. Along with nonuniformity in size, PET nanocomposites also showed less densed spherulites (Fig 2.6, 2.7, 2.8, 2.9). The color of the spherulites corresponds to the wavelength emitted from it and hence is related to the density of the spherulites. The change in spherulite shape and size was concentration dependent with 5% nanocomposite showing the maximum effect.

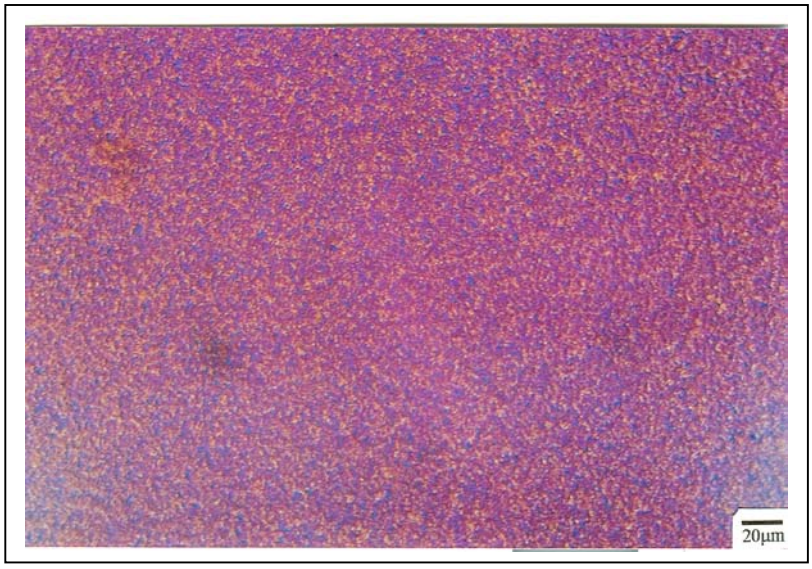

FIGURE 2.6 Polarized optical micrograph of neat PET.

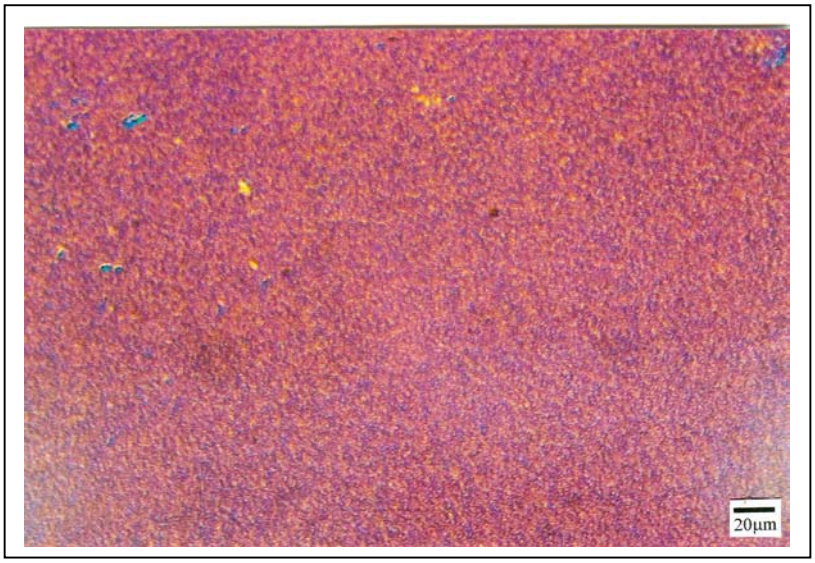

FIGURE 2.7 Polarized optical micrograph of PET + 1%MLS nanocomposite.

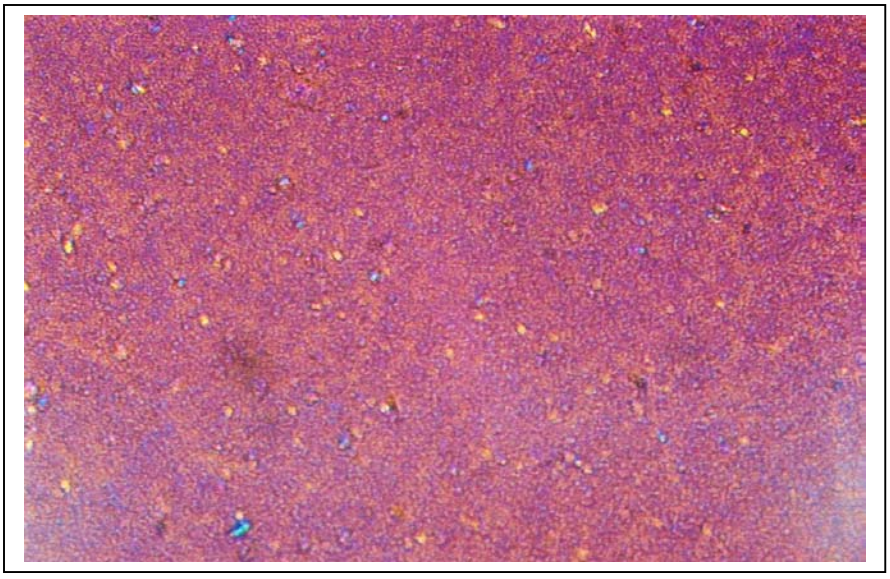

FIGURE 2.8 Polarized optical micrograph of PET + 2%MLS nanocomposite.

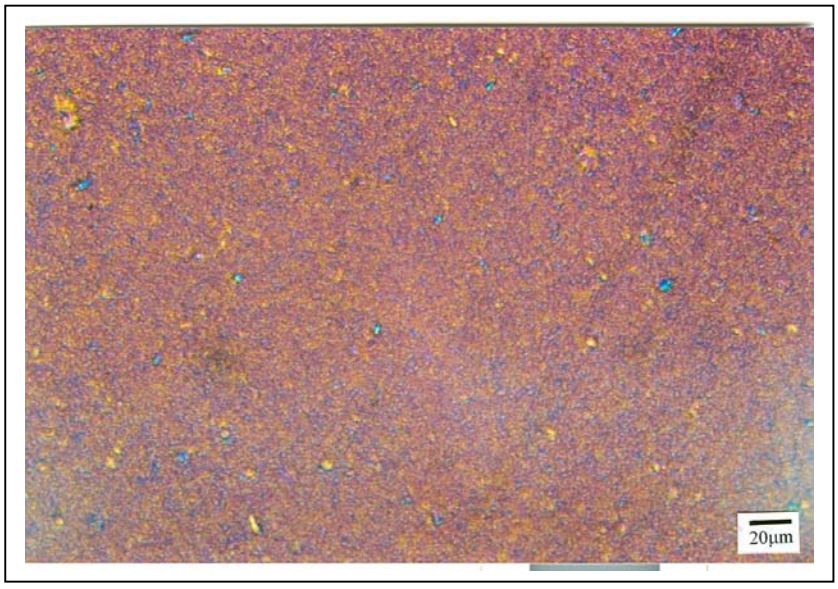

FIGURE 2.9 Polarized optical micrograph of PET + 3%MLS nanocomposite.

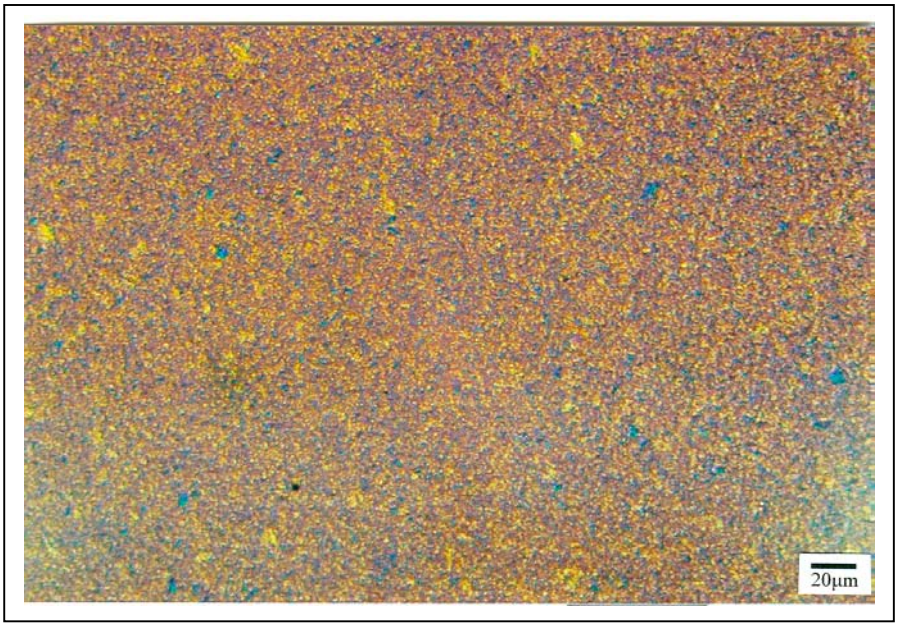

FIGURE 2.10 Polarized optical micrograph of PET + 5%MLS nanocomposite

In order to explain the non uniformity in spherulitic sizes in case of PET nanocomposites, solid liquid surface energy for different compositions was calculated using Gibb's-Thmopson equation for melting point depression[47]. The thermodynamic behavior of fluids and organic solids confined between the glassy cylindrical pores of diameter 20-500Å has been considered in this relationship. The phase bounded between the glassy confined boundaries is called as confined phase. This phase shows properties different from the bulk properties. Common observations in such studies are:

1) The melting temperature of confined solid is less than the bulk solid.

2) The melting peak of confined solid in differential scanning calorimeter analysis (DSC) shows doublet whereas the melting peak of bulk solids is a single curve.

Both these behaviors are obtained by the PET nanocomposites evident from the DSC data discussed. Hence the Gibb's-thompson equation is used.

Gibb's –Thompson equation for melting point depression(ΔTm) for crystal of size d gives the value of σsl , the solid liquid interfacial energy:

$$\Delta T_m = T_m - T_m(d) = 4\sigma_{sl} T_m / (d\Delta H_f \rho_s) \quad (2.6)$$

Tm is bulk melting temperature (Melting temperature of neat PET)

Tm (d) is melting point of crystal of size d (Melting temperature of nanocomposite)

ΔHf is bulk enthalpy of fusion (enthalpy of neat PET)

ρs is density of the solid.

Spherulitic dimensions are measured from optical microscopy by comparying the spherulitic dimensions with a predetermined scale.

The number of pixels corresponding to each spherulite corresponded with number of pixels of the scale of 20 micron.

TABLE 2.2 Calculation of solid-liquid interphase surface energy of PET nanocomposites

Composition	Tm(d) ^{o} C	d(micron)	Density (kg/m2)	σsl (mJ/m2)
KOSA+1%MLS	241	0.046	1236.8	15.3
KOSA+2%MLS	238	3.87	1093.9	2263.7
KOSA+3%MLS	239	3.51	1354	2116.1
KOSA+5%MLS	235	3.29	1332.1	3520.1

Vapor pressure of small droplets is large. If we consider various sized droplets of a pure substance, then large droplets will grow at expense of small droplets to minimize the vapor pressure. Due to confinement, the crystal size near clay surfaces decreases such that the surface energy increased significantly as apparent from above table. In order to minimize the energy, bigger spherulites grew at expense of smaller ones; hence a non uniformity in spherulite size was obtained. For 1% MLS concentration, the effect of confinement was least hence the spherulites maintain the uniformity in sizes.

2.3.3 Differential Scanning Calorimetry

Cold crystallization temperature is observed for the extruded sample i.e. it is present only in the first heat (Figure 2.11). It can be seen that as the MLS concentration increases, the cold crystallization temperature decreases with a maximum decrease for 5% MLS concentration of 35^{o} C (Table 2.3). Due to the processing history, the interspherulitic region can be more amorphous than the interlamellar region. Hence the more ordered interlamellar region undergoes crystallization giving a characteristic cold crystallization peak in PET. The results indicate that the addition of MLS has increased interlamellar order in PET.

Further heating cycles did not reveal the cold crystallization temperature. There was no cold crystallization peak irrespective of the cooling rate chosen. The fact that the cold crystallization temperature appeared only during the first heat indicates that not only the cooling rate, but other processing parameters dominate the morphology of PET and the nanocomposite. Zhang et al. (48) and Pingpang et al. (49) have found a double cold

crystallization peak in PET as a function of different annealing history, which is not observed in our system.

The addition of MLS also decreased the glass transition temperature with the, maximum decrease being 6°C for 5%MLS concentration at a cooling rate of 25°C/min. This implies that the disorder or amorphous nature increases on addition of MLS.

TABLE 2.3 Effect of Cooling Rate in Non Isothermal Crystallization of PET Nanocomposites.

MLS%	T_m^1	T_m^{45}	T_g	T_{cc}	ΔH^1(J/g)	ΔH^{45}(J/g)	T_c (onset)^1	T_c (onset)^{45}
0	244	246	67	192	87	57	230	207
1	241	244	66	178	87	63	228	208
2	238	243	66	162	78	61	225.6	207
3	239	244	65	169	84	65	226	207
5	235	243	64	157	77	60	222	204

$T_m^{1, 45}$ corresponds to melting point at cooling rates of 1^0C/min, 45^0C/min respectively.

$\Delta H^{1, 45}$ Corresponds to enthalpy of melting corresponding to cooling rates.

$T_c^{1, 45}$ is time of crystallization corresponding to cooling rate of 1^0C/min, 45^0C/min respectively

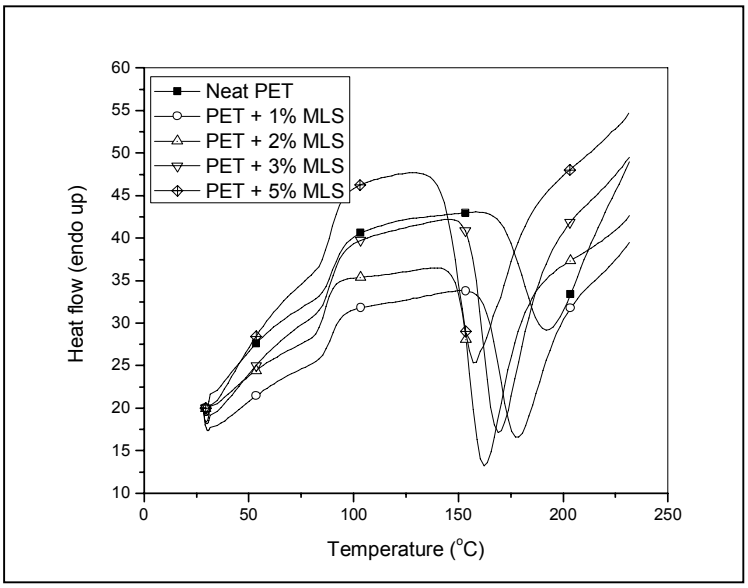

FIGURE 2.11 Cold crystallization in PET nanocomposites in first heat.

The effect of subsequent cooling cycles is analyzed further by considering 45°C/min and 1°C/min as representative rates. Figure 2.12 shows the melting thermogram of PET nanocomposites at 1^0C/min. For the cooling rate of 1^0C /min, the melting temperature of PET-1%MLS nanocomposite decreased only by 3^0C compared to neat PET (Table2.3). The decrease in melting temperature was found to be concentration dependent at low cooling rates with 5% MLS nanocomposite showing the highest drop. The decrease in melting temperature with the addition of MLS was negligible at cooling rate of 45^0C/min. A similar trend was observed during subsequent solidification. (Figure 2.13) Delayed nucleation was observed with increase in MLS concentration. The delay in nucleation was also sensitive to cooling rates with 1^0C/min showing highest delay compared to 45^0C/min. DSC analysis showed delayed nucleation due to the presence of

MLS. We correlate this effect to the dispersion observed in PET nanocomposites. A highly exfoliated dispersion was observed in 1% PET nanocomposites. After this MLS concentration, it gradually shifted to exfoliated-slightly intercalated dispersion pattern. Thus if the MLS platelets are well distributed in the matrix, then the distance between two platelets is sufficient for the polymer chains to grow. If the MLS platelets are agglomerated then due to reduced distance between the two platelets, there is no room for the chains to grow. Thus MLS puts a barrier effect on crystallization of PET chains whenever they are present in a large number. At higher cooling rates, there is insufficient time for MLS to affect the nucleation of PET. The enthalpy of crystallization shows a similar trend i.e. at a cooling rate of 45^{o}C/min. the addition of 1% MLS gives an increased enthalpy whereas higher MLS concentrations give reduced enthalpy. At lower cooling rate, on the other hand, there is a decrease in enthalpy of crystallization. This shows that the lower cooling rate provides sufficient time for interlamellar ordering or disordering to occur. This reduced enthalpy in nanocomposites suggest that there are larger chain ends, less perfect spherulites formed on addition of MLS.

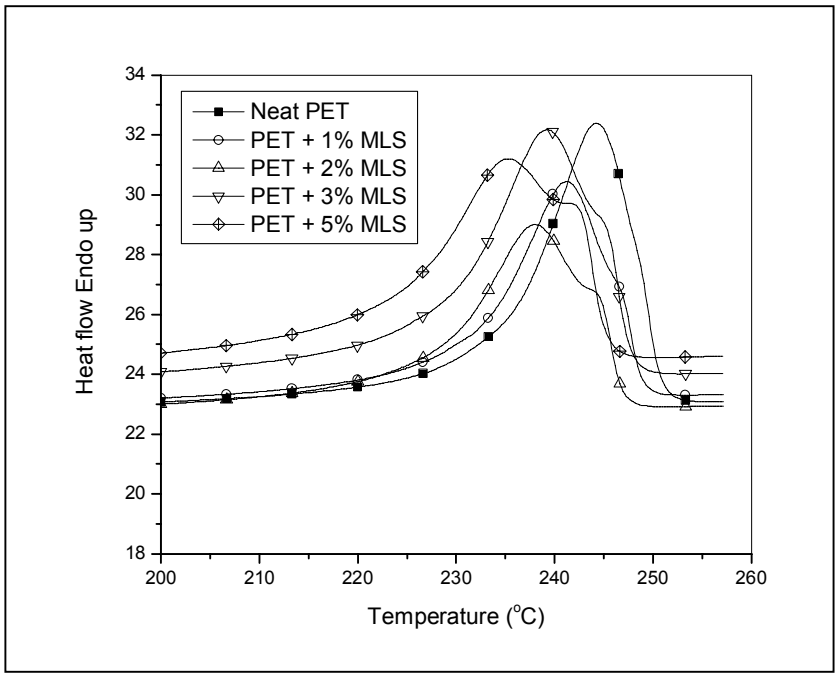

FIGURE 2.12 Heating thermogram of PET nanocomposites corresponding to cooling rate of 1°C/min.

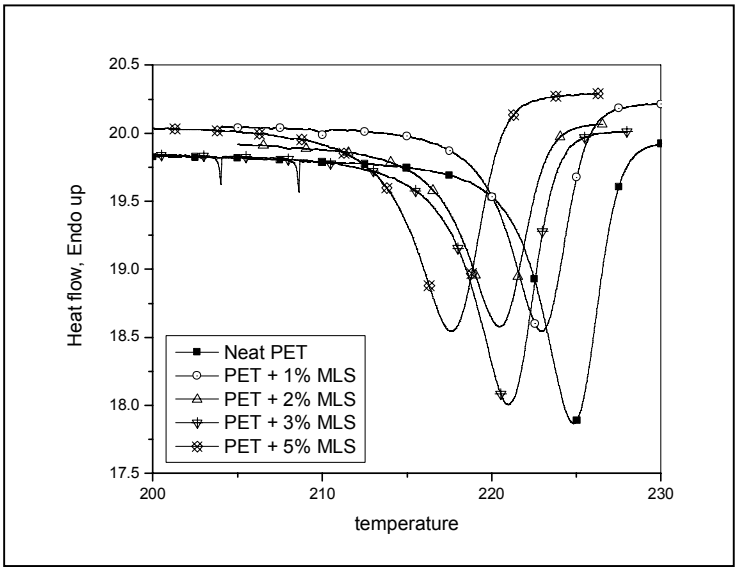

FIGURE 2.13 Cooling thermogram of PET nanocomposites.

The influence of MLS concentration and cooling rates was examined via the Avrami analysis. The temperature for crystallization to occur was taken into account and the corresponding times of crystallization were obtained from this data. For a cooling rate of 1 ^{o}C/min, the Avrami constant (n) was 1.6 for neat PET (Table 2.4). This intermediate value denotes circular lamellar geometry. This value increased on addition of MLS to 2.3. For higher cooling rate of 45^{o}C/min, the values of n were higher compared to cooling rate of 1^{o}C/min. These values remained almost constant for neat PET and nanocomposites with varying percentages of MLS. From the above observations it was concluded that higher dimension spherulites are formed with higher cooling rate with dimensions being highest at the cooling rate of 40^{o}C/min.

The rate constant (k) increased from lower cooling rates to higher cooling rate of 45^{0}C/min. This increase is almost 2200 times in case of pure PET and PET-1%MLS nanocomposite. Comparatively the increase in rate constant is less for higher MLS concentrations. This leads to the conclusion that at higher cooling rates, more nucleation sites are effective. It also proved that for higher cooling rates, after 1% MLS addition even if MLS addition is increased, the number of nuclei remains the same. A significantly exfoliated structure was obtained in PET-1%MLS addition. This resulted in a large increase in nucleation sites. For higher concentrations of MLS, the rate constant was less than even neat PET. The agglomerations of particles lead to this phenomena. A similar result has been obtained by Fornes et al. [36] in nylon nanocomposites, i.e. the rate constant shows a maximum for lower MLS percentages. Kennedy et al.[22] have studied a

syndiotactic PS-silica particle system and observe increased rate of heterogeneous nucleation on addition of silica particles. At the same time, they found decreased spherulite growth rate. They associated the silica particle as a quasicrosslink which hinders diffusion of polymer segments.

TABLE 2.4 Non-isothermal Avrami analysis for PET nanocomposite.

MLS %	n^{1}	n^{25}	n^{40}	n^{45}	k^{1}	k^{25}	k^{40}	k^{45}	tc (min)*	tc (min)**
0	1.6	2.5	3.6	2.5	0.07	12.8	33.5	153.9	18.7	0.37
1	2.3	2.3	3.4	2.5	0.03	10.0	40.7	209.5	6.3	0.35
2	2.3	2.3	3.0	2.1	0.02	9.2	19.2	68.9	6.5	0.36
3	2.4	2.6	3.3	2.98	0.02	11.4	19.9	122.1	19.6	0.40
5	2.7	2.4	2.98	2.2	0.01	7.5	13.4	59.5	6.9	0.45

$^{1, 25, 40, 45}$ = cooling rates of 1 ^{o}C/min, 45 ^{o}C/min respectively.

*, ** Corresponds to the crystallization time at cooling rates of 1 ^{o}C/min, 45 ^{0}C/min respectively.

Isothermal Crystallization

An isothermal study was carried out at different temperatures of crystallization i.e. 190, 200, 205, 210^{o}C. From isothermal crystallization, it can be seen that MLS significantly reduces the time for crystallization acting as a nucleating agent (Figure

2.14). The value of n does not show any particular trend on addition of MLS. For crystallization temperature of 190^{o}C, the Avrami constant n decreases as MLS percent increases till 3% MLS addition showing that smaller crystallites are formed. But for higher temperatures this nucleating effect of MLS is not seen. The kinetic constant (nucleation density) increases dramatically on addition of 1% MLS by 12 times and then reduces on further MLS addition (Table 2.5). The trend in k is complementary with the results of non isothermal crystallization.

Generally nucleating activity of a filler or heterogeneous particle is seen as a decrease in the value of n and increase in k. In our system, for both non-isothermal and more notably for isothermal crystallization it was seen that there is apparently no effect on n but a large effect on k i.e. 12 times increase in k on addition of MLS. At the same time, the crystallization time is reduced on addition of MLS in isothermal crystallization. In non isothermal crystallization, there is no effect on time of crystallization on addition of MLS. This can be attributed to the nature of the experiment. The results of non isothermal crystallization, being a dynamic process can be explained on the basis that since the dimensions of spherulites are not changing significantly, corresponding time of crystallization is also not varied. It could be seen that apart from nanocomposite composition, the k values are highly dependent on temperature, in isothermal conditions and cooling rate in case of non isothermal analysis. Jabarin (50) have stated that, since k values are a function of nucleation and growth rate, they are sensitive to the minute changes in temperature, which is reflected in the present study.

MLS %	$T_c(^0C)$	n	k	$t_{1/2}$	$T_c(^0C)$	n	k	$t_{1/2}$	E_a(J/mol)
0	190	2.6	1.2	0.41	200	2.2	0.2	0.69	594.2
1		1.9	12.9	0.06		2.4	12.8	0.17	1872.0
2		1.9	5.4	0.12		2.1	2.9	0.24	1371.8
3		1.8	6.3	0.10		2.1	3.4	0.22	1346.9
5		2.2	4.5	0.23		2.0	1.1	0.22	523.8

TABLE 2.5 Isothermal Avrami analysis for PET nanocomposite.

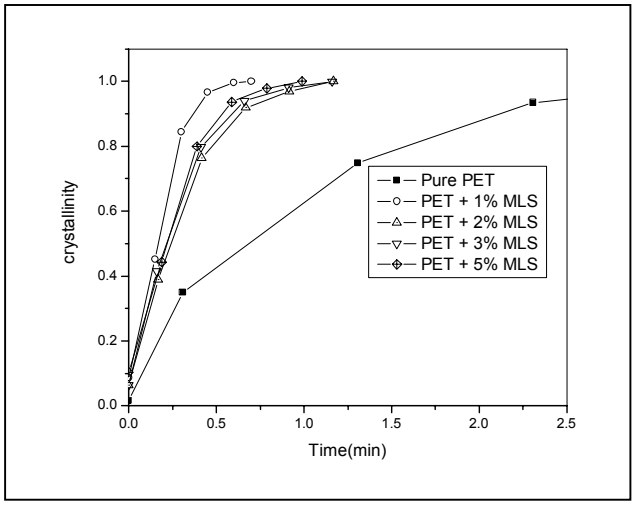

T_c= Isothermal crystallization temperature

$t_{1/2}$= half time of crystallization(in minutes)

FIGURE 2.14 Crystallinity vs. time for isothermal crystallization temperature of 200^{o}C.

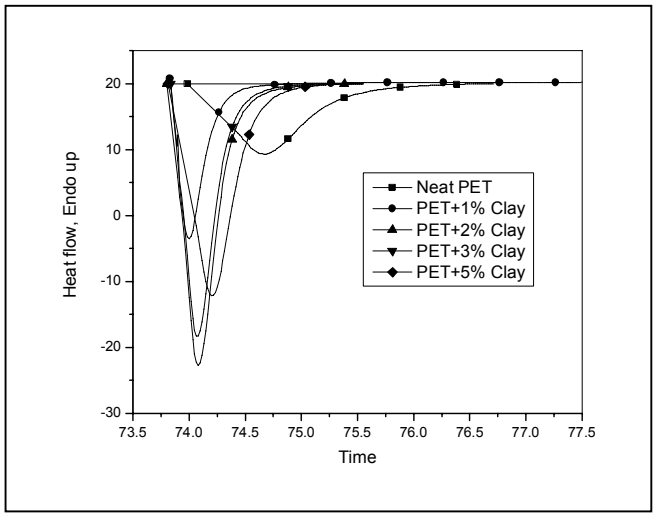

FIGURE 2.15 Crystallization curve of PET Nanocomposites at 190^0C

Activation energy of crystallization was found out using following equation to gain an insight into the ease with which crystallization occurs.

$$k_o = A_o e^{-E_a / R\Delta T} \tag{2.13}$$

Where E_o is overall activation energy. A_o is overall frequency factor. And $\Delta T = (T_\infty - T)$, the degree of undercooling from the thermodynamic equilibrium crystallization temperature T_∞ and R is the universal gas constant.

T_∞ is found out from the plot of melting temperature vs. crystallization temperature at the point of $T_c = T_m$. The results are tabulated in table 2.5. It was observed that the activation energy increased on addition of 1%MLS. This indicates that more energy is required in crystallization and hence subsequently the spherulitic changes in the optical

microscope are observed. A decrease in activation energy in 5% PET nanocomposite is also observed.

2.4 Conclusion

XRD coupled with TEM showed a highly exfoliated dispersion at 1% and 2% MLS concentration and exfoliated partially intercalated dispersion at 3% and 5% MLS concentration. At a higher cooling rate of 45^0C/min, the crystallization temperature and melting temperature remained almost the same for PET-1% nanocomposite compared to pure PET. For cooling rate of 1^oC/min, higher MLS compositions showed significant delay in crystallization temperature (8^0C) and melting temperature (9^0C). The maximum delay was for the PET-5% MLS nanocomposite. At the same time, the rate constant, k, increased with the addition of 1% MLS. This indicated that the number of nucleation sites increase. At the same time the morphology does have a negative effect seen as decreased enthalpy of crystallization and delayed melting point and crystallization temperature. The optical micrographs also depict the non uniformity in spherulites on addition of MLS. It can be concluded that the diffusion of polymer chains is affected due to the presence of MLS. This nonuniform diffusion subsequently leads to the non uniform distribution of spherulite sizes. For a cooling rate of 45^0 C/min, the changes in crystallization and melting temperatures are virtually absent. At the same time the spherulitic dimensions are unaffected due to the presence of MLS, which is depicted by Avrami constants. The rate constants increased at higher cooling rates indicating that at higher cooling rate more nucleation sites were available i.e. due to the higher

crystallization rate; the diffusion inhibition by MLS was not realized. The isothermal analysis showed a similar trend in kinetic growth constant. This result further supports the insensitivity of MLS at higher cooling rate. The cold crystallization temperature was decreased by 14^0C on addition of MLS. The presence of MLS platelets influences the interspherulitic and interlammelar order reversely manifested by decrease in glass transition temperature and cold crystallization temperature in PET matrix. The interlamellar region is more ordered showing the cold crystallization. On the other hand, the interspherulitic disorder is seen by a decrease in glass transition, melting and crystallization temperatures. Hence MLS platelets can be said to have a homogenizing effect on PET.

Since crystallinity is the factor which determines the mechanical, optical, physical and thermal properties of polymers, the above study can give useful insight on the various properties of the PET nanocomposites. One of the properties, i.e. mechanical performance is considered and discussed in the subsequent chapter.

2.5 References

[1] Figure reproduced from *Macro. Phys.*, Vol.2, B. Wunderlich, Academic Press, 1976, by permission from Elsevier.

[2] B. Wunderlich, *Macro. Phys.*, Vol.2, Academic Press, 1976.

[3] X. Lu and J. N. Hay, *Polymer*, **42**, 9423(2001).

[4] B. Wunderlich, *Macro. Phys.*, volume 1, Academic Press (1973).

[5] Figure reproduced from *Macro. Phys.*, volume 1, B. Wunderlich, (1973), by permission from Elsevier.

[6] N. Dangseeyun, P. Srimoaon, P. Suphanol and M. Nithitanakul, *Thermochimica Acta*, (2003).

[7] E. Dixon and J. Jackson, *J. of Mater. Sci.*, **3**, 464(1968).

[8] J. Jackson and G. Longman, *Polymer*, **10**,873(1969).

[9] A. Toda, M. Hikosaka and K. Yamada, *Polymer*, **43**, 1667 (2002).

[10] A. Minakov, D. Mordvintsev and C. Schick, *Faraday Discussions*, **128**, 261(2005).

[11] Z. Kiflie, S. Piccarolo, V. Brucato and F. Calleja, *Polymer*, **43**, 4487 (2002).

[12] J. Keum and H. Song, *Polymer*, **46**, 939(2005).

[13] C. Roland, *Polym. Eng. Sci.*, **31**, 849(1991).

[14] P. Chandran and S. Jabarin, *Advances in Polym. Techno.*, **12**, 153(1993).

[15] P. Verma, E. Lofgren and S. Jabarin, *Polym. Eng.Sci.*, **38**, 237(1998).

[16] S. Ahzi, A. Makradi, R. Gregory and D. Edie, *Mechanics of Mater.*, **35**, 1139 (2003).

[17] C. Heffelfinger and P. Schmidt, *J. Appl. Polym. Sci.*, **9**, 2661 (1965).

[18] Y. Marco, L. Chevalier, G. Regnier and A. Poitou, *Macromolecular Symposia*, **185**, 15 (2002).

[19] A. Taniguchi and M. Cakmak, *Polymer*, **45**, 6674(2004).

[20] B. Wunderlich, *Macrom. Phy.*, volume 2, Academic Press (1976). (and references therein)

[21] A. Somwangthanaroj, E.Lee and M. Solomon, *Macromolecules*, **36**, 2333.

[22] M. Kennedy, G.Turturro, G.Brown and L. St-Pierre, *J. Polym. Sci.: Polym. Phys.*, **21**, 1403(1983).

[23] V. Reinsch and L. Rebenfeld, *J. Appl. Polym. Sci.,* **52**, 649(1994).

[24] S. Chang and R.Shanks, *J. Appl. Polym. Sci.*, **47**, 2149 (1993).

[25] B. Wunderlich, *Macromolecular Physics*, volume 2, Academic Press (1976). (and references therein)

[26] Y. Sakaguchi, *Polymer*, **38**, 2201(1997).

[27] B. Li, J. Yu, S. Lee and M. Ree, *Polymer*, **40**, 5371 (1999).

[28] L.Liu, Z. Qi and X. Zhu, *J. Appl. Polym. Sci.*, **71**, 1133 (1999).

[29] A. Ranade, N.D'Souza,B.Gnade and A. Dharia, *J. Plastic films*, **19**, 271(2003).

[30] H. Wu, C. Tseng and F. Chang, *Macromolecules*, **34**, 2992 (2001).

[31] N. Sheng ,M. Boyce, D. Parks , G. Rutledge , J.Abes. and R.Cohen , *Polymer*, 45, 487.

[32] A. Usuki, M. Kawasumi, Y. Kojima, A. Okada, T. Kurauchi and O. Kamigaito, *J. Mater. Research*,**8**,1174(1993).

[33] A. Usuki, Y. Kojima, M. Kawasumi, A. Okada, Y. Fukushima, T. Kurauchi and Osami Kamigaito, *J. Mater. Research*, **8**, 1179(1993).

[34] Y. Kojima, A. Usuki, M. Kawasumi, A. Okada, Y. Fukushima, T. Kurauchi and Osami Kamigaito, *J. Mater. Research*, **8**, 1185(1993).

[35] V. Krikorian and D. Pochan, *Macromolecules*, **37**, 6480(2004).

[36] T. Fornes and D. Paul, *Polymer*, **44**, 3495(2003).

[37] G. Jimenez, N. Ogata, H. Kawai, T. Ogihara , *J. Appl. Polym. Sci.*, **64**,2211(1997).

[38] W. Weng, G. Chen and D. Wu, *Polymer*, **44**, 8119 (2003).

[39] T. Wan, L. Chen, Y. Chua and X. Lu, *J. Appl. Polym. Sci.*, **94**, 1381 (2004).

[40] D. Lincoln, R. Vaia, Z. Wang and B. Hsio, *Polymer*, **42**, 1621 (2001).

[41] Y. Ke, Z. Yang and C.Zhu, *J. Appl. Polym. Sci.*, **85**, 2677(2001).

[42]Y. Ke , C. Long and Z. Qi *, J. Appl. Polym. Sci.*, **71**, 1139(1998).

[43] C. Ou , M. Ho and J. Lin, *J. Appl. Polym. Sci.*,**91**,140(2004).

[44] A.Sanchez-Solis,A. Garcia and O. Manero, *Macrom. Symposia,* **192**,281.

[45] C. Davis, L. Mathias, J. Gilman, D. Schiraldi, J. Shields, P. Trulove, T. Sutto and H. Delong, *J. Polym. Sci., Part B, Polym. Phys.*, **40**, 2661 (2002).

[46] X.Hu and A. Lesser, *J. Polym. Sci., Part B, Polym. Phys.*, 41, 2275(2003).

[47] R. Defay and I. Prigogine, Surface Tension and Adsorption, Wiley (1966).

[48] Z. Zhang, M. Ren, J. Zhao, S.Wu and H.Sun , *Polymer*, **44**,2547.

[49] Z. Pinping and M. Dezhu, *European Polym. Journal*, **36**, 2471(2000).

[50] S. Jabarin, *J. Appl. Polym. Sci.*, **34**, 85(1987).

CHAPTER 3

ESSENTIAL WORK OF FRACTURE

3.1 Fracture Mechanism in Ductile Polymers

Ductile polymers undergo a transition to brittle fracture mode on modifying the polymer or changing test conditions such as rate of testing, temperature of testing etc. There are two competing mechanisms occurring during fracture, ductile shear yielding or brittle fracture mechanism such as crazing. The difference between these two mechanisms is that the shear yielding is a constant volume process whereas in crazing, the volume increases. Polymer fracture processes can be divided as follows (1):

- Excitation of bonds occurs under the action of applied stress.
- Due to thermal effects, the excited overstressed bonds break.
- Small submicrocracks or crazes occur which develop further to form larger cracks.

3.2 Essential Work of Fracture (EWF)

Linear elastic fracture mechanics (LEFM) and post yield fracture mechanics (PYFM) are two important approaches to deal with fracture toughness of polymers. LEFM considers deformation which is linear elastic and hence is restricted to brittle failure in polymers, impact tests etc. On the other hand, PYFM is of considerable importance in ductile polymers (2). For ductile polymers and their blends, two approaches of PYFM commonly used are J integral approach and essential work of fracture. For the J integral approach, certain size requirements must be met, which can not be met by thin ductile polymer films. Hence EWF approach is commonly used.

The non elastic region at the tip of a crack is subdivided into 2 regions. These include a region where the fracture process takes place and the outer region surrounding it where gross ductile yielding occurs (3). Accordingly, EWF considers two parameters. One of it is the specific essential work of fracture (w_e), which is a material constant under plane stress conditions, for a given specimen thickness. The second parameter is the specific non essential work of fracture or plastic work (w_p), which varies with the specimen geometry, gauge length etc.

The method requires that the area under load-displacement curve i.e. the energy to fracture for a series of fracture specimens is measured. This ensures that the plasticity in the ligament (fracture region) is fully developed. Hence the fracture is divided into two elements. In the first element, fracture taking place along the line of fracture, proportional to fracture area (i.e. ligament length, where fracture is concentrated. In the second element, the volume of material surrounding the crack is determined.

The total energy absorbed in fracturing any specimen is given as follows:

$$W_f = w_e.lt + w_p.\beta l^2 t \tag{3.1}$$

W_f , the total energy absorbed in fracturing the specimen

l , ligament length or region where fracture occurs

t , sheet thickness

β , shape factor associated with dimensions of plastic zone normal to crack line

Dividing the above equation with $l\ t$,

$$w_f = w_e + \beta w_p.l \tag{3.2}$$

Hence essential work of fracture is determined from the intercept of the graph of w_f against l.

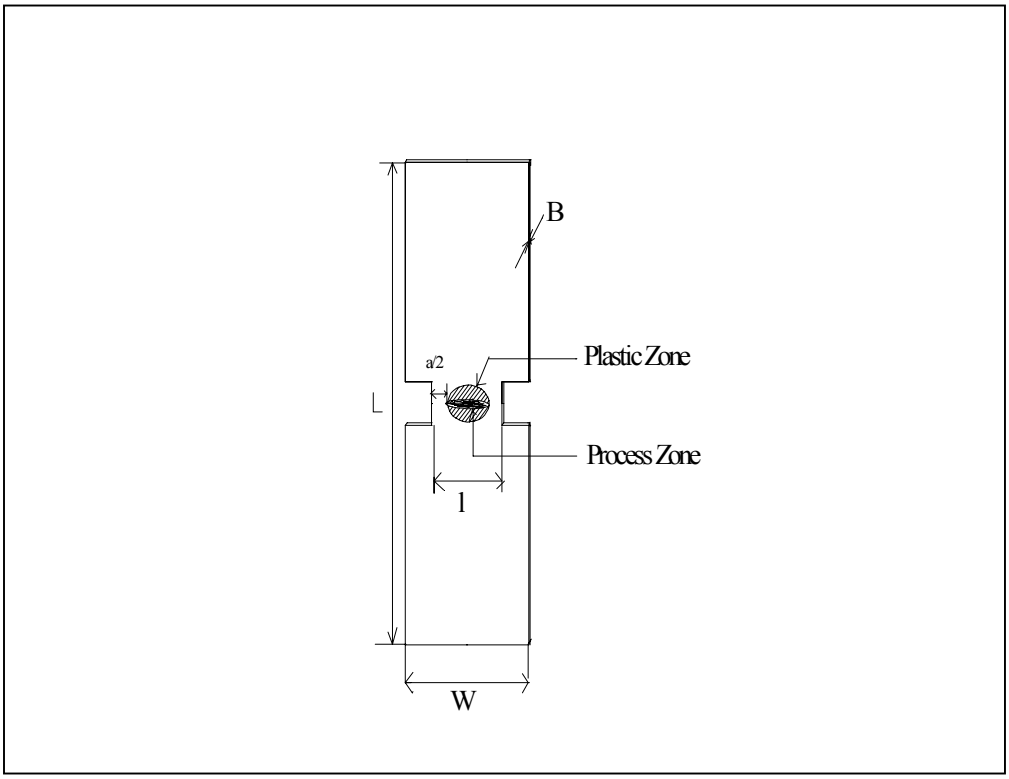

FIGURE 3.1 DENT specimen and nomenclature (4).

The value of w_e is determined in a state of plane stress and following restrictive points should be considered while choosing the geometry of the specimen for EWF:

- The ligament length, L, should be small compared with total width of sample, W. If L is large, then the size of plastic zone can be influenced by the specimen boundaries. Hence arbitrarily, a size restriction is imposed to avoid this edge effect as: $L \leq W/3$
- The size of the plastic zone should be controlled by the ligament length only. If the crack growth occurs prior to yielding of ligament, then the plastic zone is controlled by crack growth. Hence in order to ensure complete yielding of the ligament,

proportionality between Wp and L^2 should be maintained. Hence if R_p is the radius of the plastic zone at crack tip, the condition is expressed as: $L \leq 2R_p$

- Pure plane stress condition should be maintained during the testing. Hence if the ligament length is not too large compared to the thickness of the sample, B, then the condition of plane stress/plane strain arises. Hence w_e and w_p become dependent on L giving rise to non linear relationship shown as in. Hence the recommended ligament length is: $L \geq 3B - 5B$

From the above points, it can be seen that the empirical size restrictions are: $3B - 5B \leq \min(W/3 \ , \ 2R_p)$

Where,

$$R_p = (\pi / 8) \bullet (Ew_e / \sigma_y^2) / 2 \tag{3.3}$$

The other important experimental considerations which may affect the EWF results are mentioned by ESIS TC-4 committee

- The geometry used should produce similarity in the shape of the load displacement diagrams for a specific set of ligament lengths. Based on this, there are some particular geometries being used which result in stress concentration at ligament tip like deeply double notched tensile (DDEN-T) specimens, trouser specimen, dumbbell shaped specimens (5) and deep centered notched tension (DCNT) (6) etc.
- Sharpness of the notch is a contributing parameter in achieving accuracy. Also the symmetry of the notches is important. Hence Hashemi (7) have recommended

drawing a reference line at the center of the specimen to abide by the ESIS-TC4 group protocol.

- Fracture mechanism in polymers strongly depends on the rate of deformation. This is primarily due to the fact that the chain flexibility and chain entanglements are the two dominating factors, which determine the mechanical response of polymers (8). When a plastic component is tested at a higher rate of deformation, there are two competing mechanisms taking place. Due to the high rate of testing, the chains act as a rigid network. Molecular movements are suppressed as there is little time available for rearrangement of chains. On the other hand, under high test rates, there is prominent temperature rise ahead of crack tip within the plastic zone, which can facilitate molecular movement. Hence toughness of polymer depends on which of the above mechanism is dominating (9). A speed of 0.2 times the gauge length is recommended.

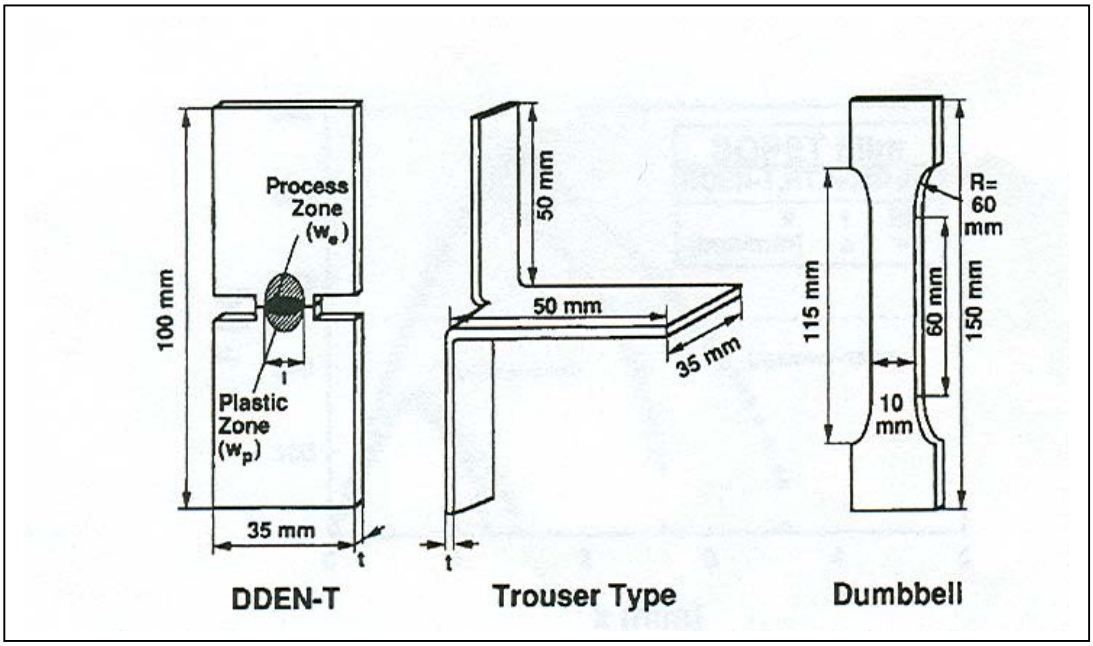

FIGURE 3.2 Typical geometries of samples used in EWF testing (10).

3.2.1 Previous Work

The different geometries shown in figure 3.2 are studied and compared for the essential work of fracture parameters extensively. Karger- Kocsis et al. (5) compared the EWF parameters obtained by mode I as well as mode III tests represented by dumbbell DDEN-T and trouser type specimens respectively in symmetrically biaxially oriented PET (BOPET) and chalk filled (filler content approximately 12%) BOPET films. Reducing the speed of testing from 20mm/min to 1mm/min did not affect the w_e values but changed βw_p noticeably. Thermal wave imaging (TWI) pictures indicated that crack growth started before the ligament fully yielded, which is a deviation from the restrictions on testing. The temperature rose by 4^oC before fracture. It was found that $w_e(\mathrm{mode\ III}) < w_e(\mathrm{mode\ I})$ due to anisotropic response in mode III. DSC and FTIR results confirmed that there was no strain induced crystallization present in the fractured samples. Hernandez-Luna et al. (11) in their study of fracture toughness of PP nanocomposites have shown a similar effect of crack growth preceding the plastic zone.

The applications of EWF method include investigation of tearing mechanism and fracture toughness (12).

3.2.2 Fracture Toughness

Value of w_e corresponds to the quantitative measurement of fracture toughness, which is the intrinsic resistance of the material to initiation of critical defects leading to fracture. Whereas the value of $\beta * w_p$ is the measure of ductility of the material. This

method is very useful to compare effect of polymer modification, either by addition of copolymer, filler or compatibilizer as discussed below.

The EWF method has been successfully used in studying the toughness mechanism of ductile polymers and their blends (13). Wu et al. (13) studied the toughening mechanism of poly (butylene terephthalate) / polycarbonate / impact modifier (PBT/PC/IM) and ABS/PC blends along with LLDPE films using both EWF approach and J integral method. They observed that the transition region of l/t for which the plane stress to plane strain transition occurs depends on the nature of the polymer and is not universal. They also observed a nonlinear relation ship between w_f and l, hence the data was fitted by extrapolation to give plane strain specific essential work of fracture w_{le}. These values were equivalent to the plane strain value obtained via J integral method. Evaluation of toughness of ductile LLDPE films by EWF approach was of importance because it can not be evaluated by any other characterization method. Similarly the effect of thickness on the EWF as well as J integral parameters was studied by Levita et al. for of rigid PVC (14).

The effect of a compatibilizer on the toughening mechanism of blend has also been studied extensively. Mouzakis et al. (15) studied the effect of glycidyl methacrylate (GMA) containing a modifier on the fracture toughness of PET-grafted ethylene propylene rubber blend. The essential and non essential work both decreased on increasing the modifier. For a particular composition of 10% modifier, the deviation in this trend was observed due to finely dispersed blend. But attempts to reproduce this result failed indicating the processing dependence of this effect and subsequent

morphology observed. They observed that 9 months of aging of the samples leads to decrease in toughness and a transition towards brittle fracture took place due to aging effect.

The effect of molecular structure on EWF was observed in amorphous PET (aPET), copolyesters containing cyclohexylenedimethylene (aPET-C) and neopentyl glycols (aPET-N) (9). At higher deformation rates, aPET-C and aPET-N showed a ductile-brittle transition zone, whereas fracture in aPET remained in the ductile zone. This effect was attributed to molecular entanglement. At 1000mm/min, there was 30^{o}C rise in temperature affecting the molecular mobility in a positive way. At high deformation rates of 500mm/min and 100mm/min, strain induced crystallization was evident from optical microscopy and WAXD, which can contribute to higher w_e at increased deformation rates. This effect of deformation rate is different in different polymers. DMA analysis of aPET proved that the fracture of a specimen at deformation rate of 100mm/min was completed at temperature between α and β relaxation corresponding to a temperature rise of 35^{o}C.

Similar to blends, organic fillers also affect the mechanical properties of polymer. Effect of incorporation of MLS on fracture toughness of polymer nanocomposites has been studied as these nanocomposites are used in structural applications. Reduced toughness in PP nanocomposites was reported by Bureau et al. (16). They compared the toughness in pure PP with that of 2 types of MLS having different degrees of hydrophilicity and also the influence of incorporation of 2 types of coupling agents. The improvement in tensile properties was attributed to high aspect ratio in nanocomposites.

However in case of PP with more hydrophilic nanocomposite the fracture toughness was reduced significantly, 75% reduction in w_e value. The fracture surface micrographs indicated extensive void nucleation in case of this hydrophilic clay containing nanocomposite. The particle-polymer matrix adhesion was very limited. This resulted in a void nucleation and led to decreased toughness in nanocomposites. At the same time, they observed an increase in plastic yielding, which was attributed to extensive fibrillation occurring in nanocomposites. The addition of 2 types of coupling agents increased the toughness in nanocomposites due to better platelet-matrix adhesion as well as increased plastic yielding. Both the coupling agents had similar effects on the matrix. Thus the platelet- matrix adhesion was considered as the key in the toughening mechanism in polymer nanocomposites. The effect of addition of maleic anhydride addition on the toughening mechanism of PP nanocomposites was studied with PP nanocomposites having a similar failure mechanism as that of the neat PP. The difference being that polymer nanocomposites showed an additional failure mechanism of interface debonding (17). The addition of low molecular weight and more highly crystalline compatibilizer than the matrix contributed negatively to the fracture toughness. This was because the addition of MLS introduced flaws in the PP matrix that intensified the applied stress at the flaw tip. It was also hypothesized that the addition of impact modifier (here, maleic anhydride) induced other failure mechanisms as rubber cavitation and interfacial debonding. The rubber modifier also absorbed some energy and reduced the stress intensity of the crack.

Addition of rubber modifier has been seen as the method to increase fracture toughness in brittle polymers. In polyamide-MLS nanocomposites, brittle fracture was determined from tensile testing (18). The MLS was organically treated in the laboratory. To enhance the toughness of these polyamide nanocomposites, a rubber modifier was added to the system and fracture toughness measured with the help of EWF. Styrene-ethylene butylenes- styrene (SEBs-g-MA) - polyamide-MLS blend was prepared via melt compounding. Both the essential as well as non essential work increased on addition of modifier. This was mainly because of crack arrest occurring at the second SEBS-g-MA phase. Thus addition of this modifier was seen as the means of optimizing properties in polymer nanocomposites in terms of toughness and stiffness.

The fracture mechanics of PP and nylon nanocomposites was compared which represent different bonding of polymer chains to the MLS platelets (19). Nylon-MLS nanocomposite being obtained by in situ polymerization had a high adhesion and PP-MLS by melt intercalation had a weak interface. At room temperature, the nylon nanocomposites have a very brittle behavior. Above the T_g, on the other side, the reinforcing effect of MLS is realized in terms of yield stress values twice as high for the nanocomposite. The fractograph of nylon nanocomposite showed that due to the high polymer-MLS interaction, the localized damage at the polymer-MLS platelet interphase caused the cavitation and fibrillation. In PP nanocomposites, at room temperature, both the pure PP as well as nanocomposites exhibited almost similar ductility. The fractograph also showed some cavitation and fibrillation, although the extent of these phenomena was

found to be larger in case of nylon nanocomposites. Hence the interaction between the matrix and MLS platelets was the key in the fracture mechanism.

Fracture mechanism of PP nanocomposites was investigated with J integral approach wherein maleated PP was used as the matrix (20). The MLS was organically treated and melt blended in ratios ranging from 5% to 50%. The mechanical properties showed an increase in the yield strength for MLS content of 40 wt %. The ductile to brittle transition was observed as there was gradual increase in clay loading. Till MLS loading of 10%, the fracture shows extensive fibrillation. At higher loadings, premature voiding of the fractured surface was obtained in the fractograph. Surprisingly, they observed that 10 and 20 wt% MLS nanocomposite systems showed substantial resistance to crack propogation. This was attributed to a reduction in mobility at high loadings and the confined intercalated structure of the nanocomposite system. The debonding at the polymer clay interface at the point of fracture further prolongs time to fracture by a providing a closure force. This indicates the unique role of interface in nanocomposite.

EWF was applied in studying the nanostructured polymer materials, polystyrene-polybutadiene block copolymer/homopolymer blends (21). The resistance against stable crack initiation and growth was found to be a strong function of the morphology of the materials. The properties of the butadiene-styrene star block copolymer (ST3) were compared with ST3-PS blend. It was found that the highly ductile ST3 is transformed into a brittle and stiff ST3-PS blend.

3.3 Experimental

3.3.1 Film Processing

PET nanocomposite films of around 10-mil thickness were prepared on a Thermo Haake Polydrive single screw extruder with a film die attached. All samples were dried overnight in a vacuum oven at 80^{o}C prior to every run. Films were collected on chilled rolls set at a temperature of 20^{0}C.

3.3.2 Tensile Testing

A MTS 810 hydraulic system was used to measure PET nanocomposite film properties. ASTM standard- D882-95a was used to perform the testing. For essential work of fracture, geometry of the film was selected according to suggestions by ESIS TC-4 committee as shown in the figure 3.1. L, ligament length equal to 70mm, width (W) equal to 35mm and ligament length ,l, as 5mm, 11mm and 17 mm . The symmetry of the notches was achieved by drawing a center reference line initially. The notch was cut by a new sharp razor blade in a smooth stroke. The sample geometry selected is referred as DENT (double notched tensile specimen). The speed of testing initially selected was 1mm/sec and 10mm/sec.

3.3.3 IR Thermography

For the thermal imaging, Prism DS infra red camera from FLIR systems was used. It has a platinum silicide IR detector with accuracy of 2% of the range. The camera was placed as close as possible from the stretched sample surface.

3.4 Results and Discussion

Tensile testing was done before the essential work of fracture test was carried out. The yield strain in pure PET was 65% more than PET nanocomposites. At the same time the yield stress in pure PET was also higher. The presence of MLS imparted stiffness to the PET matrix. The strain reduction was found as MLS tactoids acted as a stress concentration area facilitating the fracture of the sample. Any further addition of MLS does not seem to affect the strain. The results of tensile test are tabulated below:

TABLE 3.1 Results of tensile testing of PET nanocomposite.

Composition	Yield load (N)	Yield stress (MPa)	Yield strain (%)	Elastic modulus (GPa)	UTS (N)
Pure PET	21.3	43.5	2.3	2.0	28.8
PET + 1%MLS	19.8	36.7	1.4	2.6	25.9
PET + 3%MLS	16.9	35.2	1.5	2.3	23.7
PET + 5%MLS	18.3	36.0	1.5	2.5	24.8

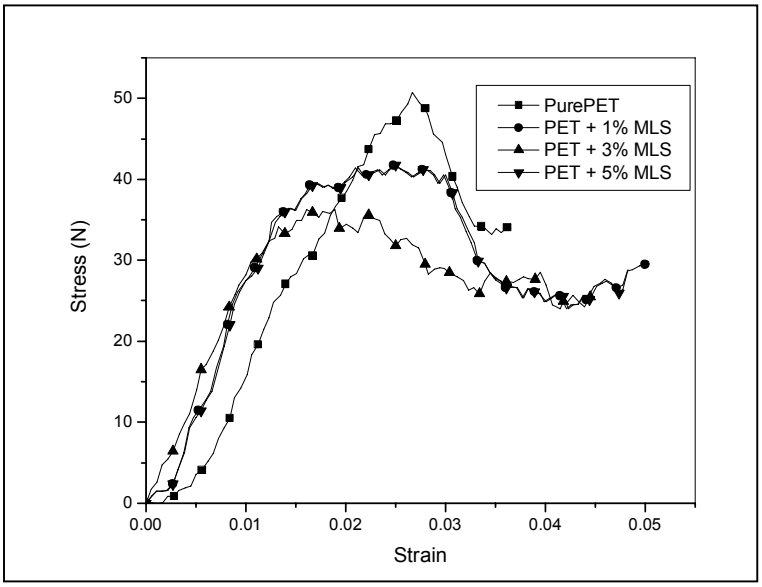

FIGURE 3.3 Tensile test data of PET nanocomposites.

3.4.1 Essential Work of Fracture

The effect of the addition of MLS on the fracture behavior is studied by considering the nature of the load vs. displacement curves. Figure (3.4) and (3.5) indicate the load-displacement curves at different ligament lengths for pure PET and PET + 3%MLS nanocomposite films for different ligament lengths. For each ligament length, samples were tested till 3 consistent readings were obtained. This is mainly due to the large variation in sample properties which is also reported by Maspoch et al. (22) in biaxially oriented PET films. The nature of these load-displacement curves for different ligament lengths is similar. This is one of the preconditions for EWF to be valid.

Also notable differences between the fracture behavior of pure PET and PET + 3%MLS were observed. In pure PET, for all the ligament lengths, there is an initial

increase in load with displacement which is subsequently followed by a large amount of plastic deformation. The initial increase is said to be recoverable on unloading. The region after the maximum in the curve showed strain softening which is seen as the fall in the true stress value past yield point. Strain softening is an intrinsic property of material and hence is observed inspite of the ligament length used. In case of 3% PET nanocomposite, there is a gradual increase in load, followed by brittle fracture of the sample. Brittle fracture initiated by crazing was correlated with inorganic dust particles trapped in the polymer. The crazing appears as stressed whitened region perpendicular to the maximum stressed direction. Hence the inorganic clay particles, particularly the tactoids or agglomerates of the MLS, initiated the crack in 3% PET nanocomposite causing brittle failure. Crazes initiate, grow and break down to give cracks at stresses below to substantially yield cause the bulk shear yielding and hence result in brittle fracture. The low strain and stress for craze initiation results in low value of fracture energy. Hence the work of fracture was much less in 3% PET nanocomposite as opposed to the pure PET. This observation is substantiated by calculation of EWF parameters discussed below.

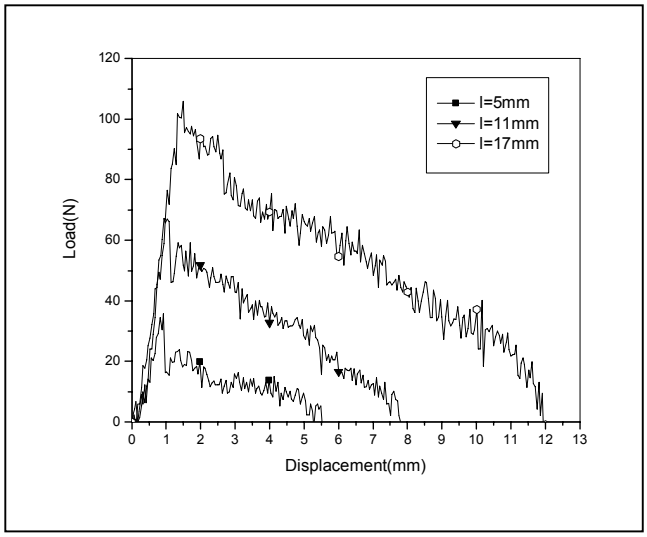

FIGURE 3.4 Graph of load vs. ligament length for pure PET.

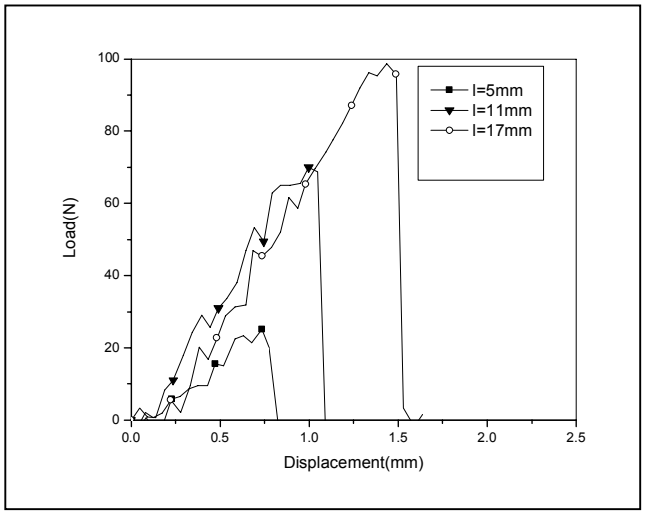

FIGURE 3.5 Graph of load vs. ligament length for PET + 3%MLS.

The 3% PET nanocomposite was tested at different ligament lengths of l = 5,11,17,19 mm. From the graph of w_f vs. l (figure3.6), it was observed that the linear relationship between w_f and l was obtained for ligament lengths till l = 17mm. Hence the range of ligament length between 5mm and 17mm was fixed based on this basis.

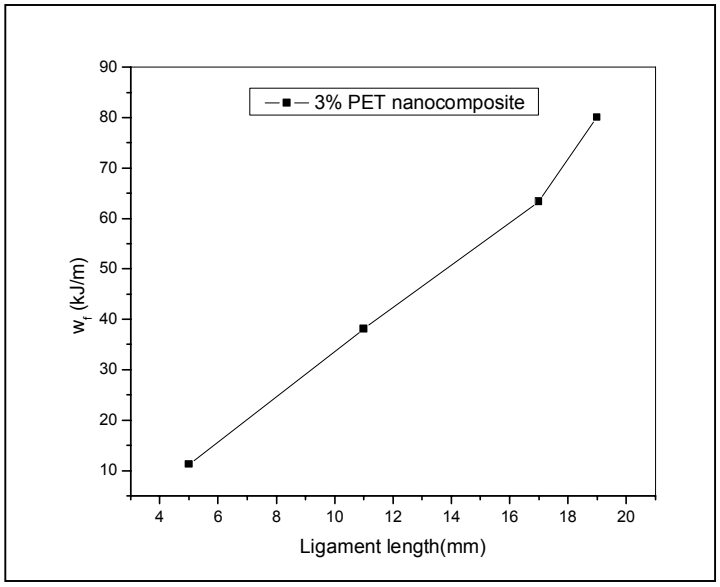

FIGURE 3.6 Graph of w_f vs. ligament length for PET+3%MLS.

Figure (3.7) shows the plot of w_f vs. l for pure PET and 3% PET nanocomposite. A linear relationship was observed for both compositions. The slope of the graphs denotes the values of βw_p. These values were found to be equal to 41.9 kJ/m for pure PET and 4.4 kJ/m for the 3% PET nanocomposite. Hence as was seen by the load-displacement curves (figure 3.4 and figure 3.5), pure PET exhibited large plastic deformation as opposed to the 3% nanocomposite. The intercept of the graph, which equals w_e, was found to be equal to 28kJ/m in case of pure PET and 4kJ/m in case of 3% PET nanocomposite. Thus it was noted that the nanocomposites also facilitate formation of new surfaces and crack as opposed to pure PET. The presence of MLS tactoids strongly correlates with this effect. The tactoid did not absorb the energy as a rubber additive would, due to its stiffness. At the same time, MLS platelets, being in agglomerated form, effectively prohibit homogenous yielding of the matrix. Yielding is

an important mechanism in improving toughness as discussed earlier. Hence the reduction in yielding also ultimately yields the brittle failure in nanocomposites.

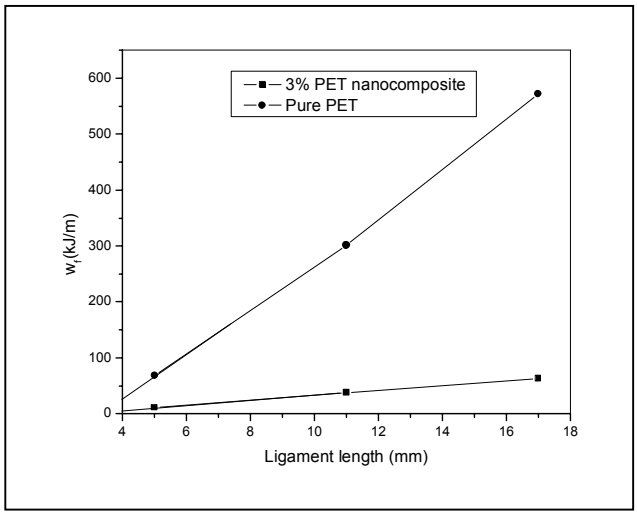

FIGURE 3.7 Graph of w_f vs. ligament length.

Morphological correlation to the crystallinity was established by DSC. Pure PET samples for ligament lengths of 11mm and 17mm were chosen. The apparent stretched film between the notches was cut and used for DSC. Figure (3.8) shows the plot of DSC of the fractured sample in comparison with the unfractured film. It was observed that the melting peak had no noticeable changes in case of fractured PET. Also, there was no effect on enthalpy of melting. But at the same time the cold crystallization peak, which was present in unfractured sample is completely absent. Hence it was seen that the stretching had no significant effect on the crystalline region of PET. However the amorphous interspherulitic region was ordered and it was manifested as a complete absence of cold crystallization peak in fractured PET samples.

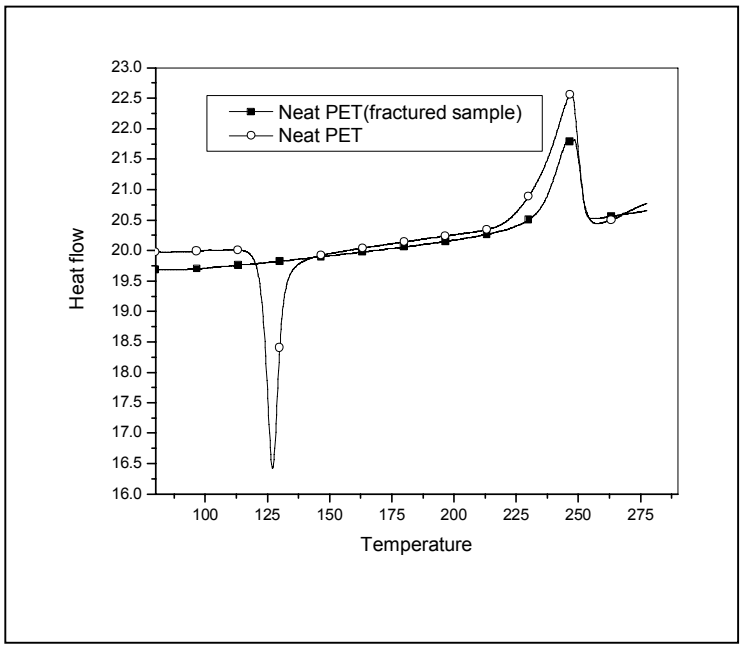

FIGURE 3.8 DSC of the deformed and non deformed pure PET sample.

3.4.2 IR Thermography

The temperature changes occurring signify the crystallization process which might be taking place on stretching. The temperature rise due to the shear of polymer molecule chains during deformation also enhances the mobility of chains. And hence temperature rise can provide a toughening mechanism. The sequential IR images captured also provide the visual representation of the plasticity developed in the polymer sample. Figure 3.9(a, b, c, d) shows the sequential IR images taken. The IR camera was focused at the notch of the specimen loaded in the jaw, and as the sample was getting pulled, real time images were captured.

The initial figure (3.9a) shows the sample before deformation. The notch geometry can be observed clearly against the dark background. The blue colored zone indicates the sample. As the sample is getting deformed, a red colored zone which

represents the plastic deformation region is identified. The red zone indicates a difference of temperature which can be read by the scale. With aid of extensive calibration, and a MatLab program (see appendix for the details of program), the change in the area of the plastic zone was calculated. There is a significant increase in the area as sample is elongated in case of pure PET, and area changes are tabulated in table (3.1).

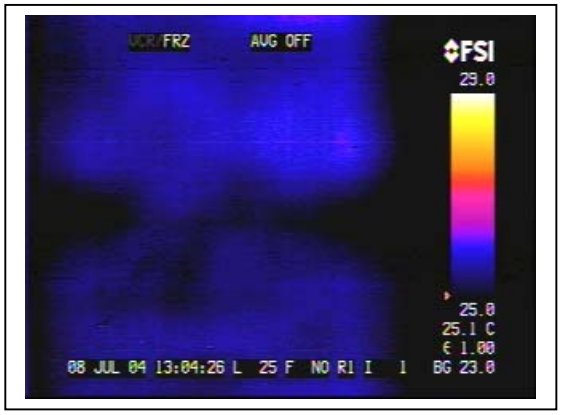

FIGURE 3.9a IR image of pure PET sample before deformation (t=0sec).

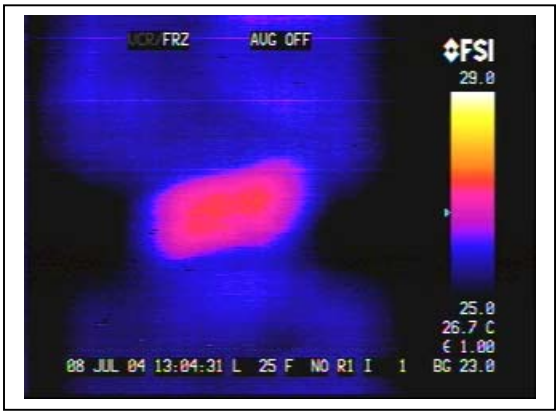

FIGURE 3.9b Pure PET sample showing plastic zone (t=4sec).

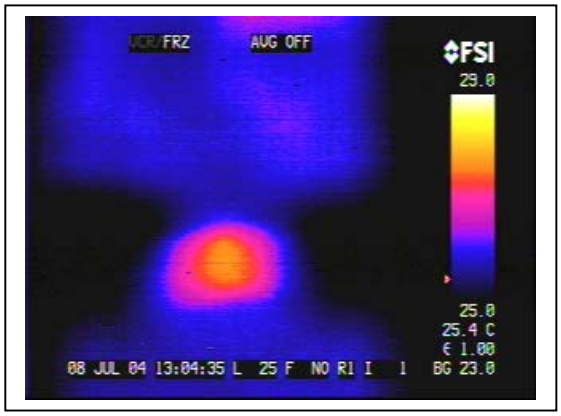

FIGURE 3.9c Pure PET sample showing plastic zone (t=8sec).

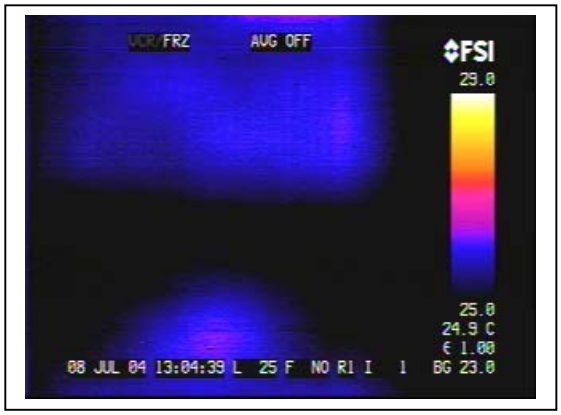

FIGURE 3.9d Pure PET sample failure (t= 12sec).

TABLE 3.2 Plastic zone area developed as pure PET sample is getting deformed (calculated with aid of MatLab program.).

Picture specification	**Stressed area(mm^2)**
Figure no 3.9 a	0
Figure no 3.9 b	0.3
Figure no 3.9 c	150.5
Figure no 3.9 d	91.0

Also the temperature profile across the fracture interval was plotted as shown in figure 3.10. There was a temperature rise of 1.6^{o}C in the initial linear stretching curve,

which facilitates the molecular movement. This rise of the temperature indicates strain induced crystallization, which was confirmed by DSC by absence of cold crystallization peak in stretched sample which was present earlier. At the same time, it was evident from both the temperature change data and the mechanical results that no major phase transition occurred.

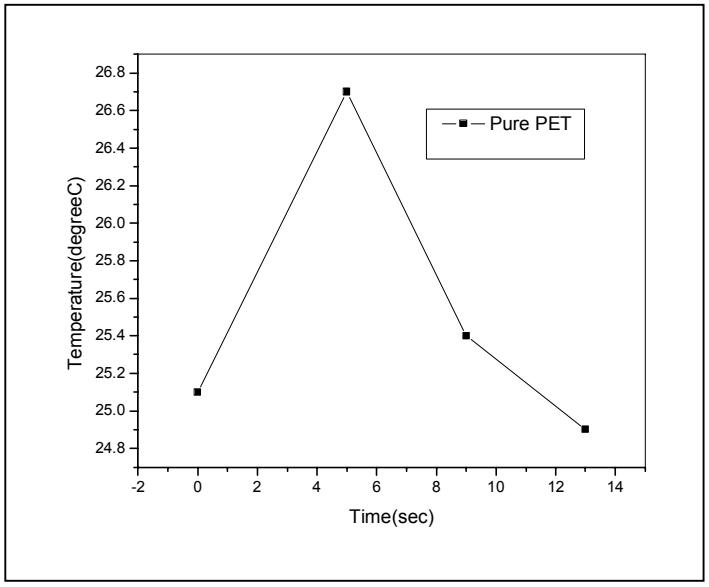

FIGURE 3.10 Temperature profile as pure PET is getting deformed.

In 3% PET nanocomposites however, the insignificant amount of plastic deformation was observed, which confirmed the mechanical analysis results. This can be clearly seen from 3.11 (a, b). There were no major temperature changes taking place in deformation of 3% PET nanocomposite.

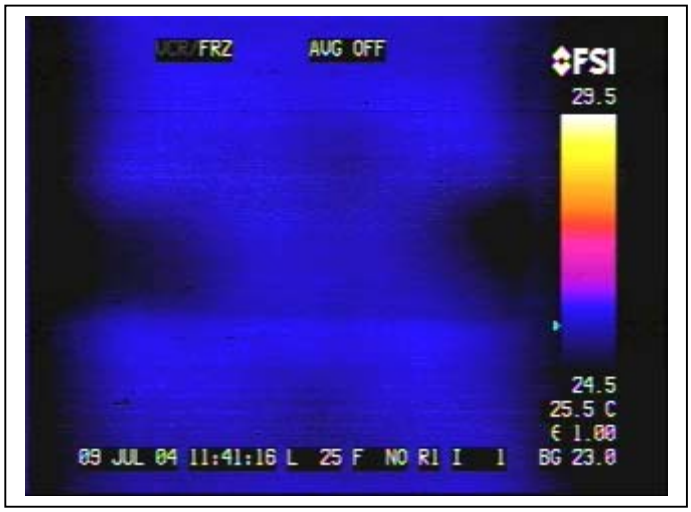

FIGURE 3.11a IR thermograph of 3% PET nanocomposite sample getting stretched (t=0sec).

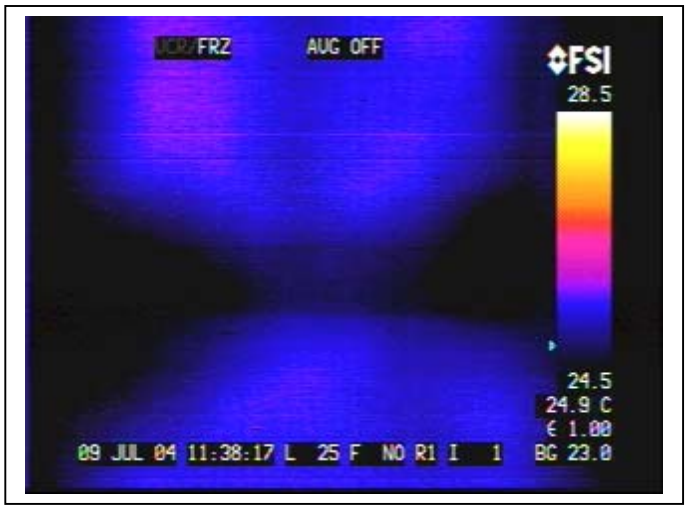

FIGURE 3.11b IR thermograph of 3% PET nanocomposite sample failure (t=4sec).

3.5 Conclusion

From previous results, incorporation of MLS in PET matrix caused non uniformity of spherulitic shape as opposed to pure PET. It was also seen that the spherulites formed in nanocomposites had defects compared to the pure PET matrix. The dispersion analysis also indicated the presence of some tactoids present in the PET matrix in 3% PET nanocomposites due to its slightly intercalated-exfoliated structure. The non uniform matrix with MLS agglomerates shows a decrease in essential as well as non essential work of fracture compared to pure PET. The essential work of fracture in pure PET is 7 times larger than that of 3% PET nanocomposite. Similarly the plastic work was larger in pure PET. From the DSC, it was observed that the cold crystallization temperature present in the non deformed sample was completely absent on stretching the sample. There was no apparent effect on the melting temperature. This proves that deformation increases order in the amorphous region.

The IR thermography results gave a visual representation of the deformation mechanism. The plastic zone developed in pure PET raised the temperature upto maximum of 1.6^{o}C. This temperature facilitated the molecular mobility providing a large toughening mechanism in pure PET. In case of 3% PET nanocomposite, on the other hand, there was no temperature change taking place.

It is concluded that pure PET had shear deformation with the plastic zone developing before fracture. In 3% PET nanocomposites catastrophic failure took place by crazing. Hence in pure PET the homogenous matrix helped in the toughening mechanism.

3.6 References

[1] A. Kinloch and R. Young, Fracture Behavior of Polymers, Elsevier (1983).

[2] J.G. Williams , Introduction To Linear Elastic Fracture Mechanics, Fracture Mechanics Testing Methods for Polymers Adhesives and Composites, Elsevier 2001, p3.

[3] E. Cluton, Essential Work of Fracture, Fracture Mechanics Testing Methods for Polymers Adhesives and Composites, Elsevier 2001, p177(and references therein).

[4] Figure reproduced from Polymer, **45**,H.Chen, J. Karger-Kocsis and J.Wu, 6375(2004), by permission from Elsevier.

[5] J. Karger-Kocsis and T. Czigany, Polymer, **37**, 2433(1996).

[6] Y. W. Mai and P. Powell, J. Polym. Sci., Part B, Polym. Phys., **29**, 785(1991).

[7] S. Hashemi, Polym. Eng. Sci., **40**, 798(2000).

[8] R. Deanin, Polymer Structure, Properties and applications, Cahners Books (1972).

[9] H.Chen, J. Karger-Kocsis and J.Wu, Polymer, **45**,6375(2004).

[10] Reproduced from Polymer, **37**, J. Karger-Kocsis and T. Czigany, 2433(1996), by permission from Elsevier.

[11] A. Hernandez-Luna and N. D'Souza, ANTEC, 1342(2003).

[12] J. Wong, D. Ferrer-Balas, R. Li, Y. W. Mai, M. L. Maspoch and H. J. Sue, Acta Materialia, **51**, 4929(2003).

[13] J. Wu and Y. W. Mai, Polym. Eng. Sci., **36**, 2275(1996).

[14] G. Levita , L. Parissi, A. Marchetti and L. Bartlommei, Polym. Eng. Sci., **36**, 2534(1996).

[15] D. E. Mouzakis, N. Papke, J.S. Wu and J. Karger-Kocsis, J. Appli. Polym. Sci., **79**, 842(2001).

[16] M.N. Bureau, F. Perrin-Sarazin and M. Ton-That, Polym. Eng. Sci., **44**, 1142 (2004).

[17] J. Zhao, H. Pham, R. Fibiger, E. Garcia-Meitin, L. Liu, V. Juarez, K. Bouchard, W. Mathews and G. Esparza, Polyolefins conference, 2005.

[18] S. Tjong and S. Bao, J. Polym. Sci., Part B, Polym. Phys., **43**, 585 (2005).

[19] J. Gloaguen and J. Lefebvre, Polymer, **42**, 5841 (2001).

[20] L. Chen, S. Wong and S. Pisharath, J. Appli. Polym. Sci., **88**, 3298 (2003).

[21] R. Lach, K. Schneider,R. Weidisch, A. Janke and K. Knoll, European Polym. J., **41**, 383 (2005).

[22] M.L. Maspoch,V. Henault,D. Ferrer-Balas,J. I. Velasco and O.O. Santana, Polym. Testing, **19**, 559(2000).

CHAPTER 4

CONCLUSIONS

1 Introduction

Semicrystalline polymer PET was melt processed with the nanoclay, montmorillonite layered silicate (MLS) in concentrations of 1, 2, 3 and 5 weight percent. Subsequent effect on the crystallization and nucleation properties of PET was studied.

Previous study shows that the dispersion of the MLS was concentration dependent. From XRD and TEM results it was proved that PET + 1%MLS nanocomposites showed complete exfoliation. Any further addition of MLS decreased the state of dispersion. A gradual transition from exfoliated to intercalated state of dispersion was seen for PET + 3% MLS. And PET + 5% MLS showed higher level of agglomeration.

2. Morphology Change

Polarized optical microscopy (POM) of pure PET showed uniform spherulites. At PET + 1% MLS, this uniformity is still maintained. But at the same time presence of less dense, non uniform spherulites also start to appear in the matrix. Further addition of MLS gradually increases such defective spherulites, the amount of defective spherulites being directly proportional to the MLS concentration. Hence crystallization behavior is studies further more with the help of DSC.

3. Hindered Crystallization

In non isothermal crystallization, at the cooling rate of 1^{o}C/min, the melting temperature as well as the crystallization temperature decreased on addition of MLS. The maximum delay of 9^{o}C/min in melting temperature and 8^{o}C/min in crystallization was observed in PET + 5%MLS. At the same time the enthalpy of melting also decreased. This supported the results of optical microscopy that MLS created more defective crystals which melted at a lower temperature. A doublet in the melting peak also showed the presence of such two forms of spherulites.

The effect of MLS on the nucleation and the spherulitic growth was further separated by Avrami analysis. It does not show any significant change in the shape of the spherulite as the function of MLS concentration. The rate constant decreased on increasing the MLS concentration. It can be concluded that the diffusion of polymer chains is affected due to the presence of MLS. This nonuniform diffusion subsequently leads to the non uniform distribution of spherulite sizes evident from both the DSC and POM results.

At the higher cooling rates of 45^{o}C/min, however, the melting point depression is not as much as compared to lower cooling rate on addition of MLS. The rate constant from Avrami analysis are also higher indicating that the hindrance due to MLS platelets is not realized at higher cooling rates.

This indicates that in the dynamic processes like extrusion molding of PET, this hindered crystallization effect will not pose an issue. The effect of this morphology was studied on fracture toughness.

4. Fracture Toughness

Pure PET showed ductile fracture with large plastic deformation region before the fracture. On the other hand, PET + 3%MLS nanocomposite showed brittle failure with almost no plastic deformation before the fracture. The essential work of fracture in case of pure PET is 7 times larger than that in case of 3% PET nanocomposite. Similarly the plastic work was larger in case of pure PET. The IR thermography results also supported these conclusions. The MLS platelets acting as the stress concentration area facilitated the propagation of crack and therefore showed failure by crazing.